Brain, Behavior, and Immunity xxx (2015) xxx–xxx

Contents lists available at ScienceDirect

Brain, Behavior, and Immunity

journal homepage: www.elsevier.com/locate/ybrbi

Toxic role of prostaglandin E_2 receptor EP1 after intracerebral hemorrhage in mice

Xiaochun Zhao [a,1], Tao Wu [b,*,1], Che-Feng Chang [a,1], He Wu [c,1], Xiaoning Han [a], Qian Li [a], Yufeng Gao [a], Qiang Li [a], Zhipeng Hou [d], Takayuki Maruyama [e], Jiangyang Zhang [d], Jian Wang [a,*]

[a] Department of Anesthesiology and Critical Care Medicine, The Johns Hopkins University School of Medicine, Baltimore, MD 21205, USA
[b] Stroke Center, Stroke Screening and Intervention Base, Changhai Hospital, Second Military Medical University, Shanghai 200433, China
[c] Department of Pathology, First Clinical Hospital, Harbin Medical University, Harbin 150001, China
[d] Department of Radiology, The Johns Hopkins University School of Medicine, Baltimore, MD 21205, USA
[e] Project Management, Discovery and Research, Ono Pharmaceutical Co. Ltd., Mishima-gun, Osaka 618-8585, Japan

ARTICLE INFO

Article history:
Received 9 October 2014
Received in revised form 28 January 2015
Accepted 8 February 2015
Available online xxxx

Keywords:
Diffusion tensor imaging
Hemoglobin
Inflammation
Intracerebral hemorrhage
Magnetic resonance imaging
Matrix metalloproteinase
Prostaglandin EP1 receptor
Src-kinase

ABSTRACT

Inflammatory mechanisms mediated by prostaglandins may contribute to the progression of intracerebral hemorrhage (ICH)-induced brain injury, but they are not fully understood. In this study, we examined the effect of prostaglandin E_2 receptor EP1 (EP1R) activation and inhibition on brain injury in mouse models of ICH and investigated the underlying mechanism of action. ICH was induced by injecting collagenase, autologous blood, or thrombin into the striatum of middle-aged male and female mice and aged male mice. Effects of selective EP1R agonist ONO-DI-004, antagonist SC51089, and nonspecific Src family kinase inhibitor PP2 were evaluated by a combination of histologic, magnetic resonance imaging (MRI), immunofluorescence, molecular, cellular, and behavioral assessments. EP1R was expressed primarily in neurons and axons but not in astrocytes or microglia after ICH induced by collagenase. In middle-aged male mice subjected to collagenase-induced ICH, EP1R inhibition mitigated brain injury, brain edema, cell death, neuronal degeneration, neuroinflammation, and neurobehavioral deficits, whereas its activation exacerbated these outcomes. EP1R inhibition also was protective in middle-aged female mice and aged male mice after collagenase-induced ICH and in middle-aged male mice after blood- or thrombin-induced ICH. EP1R inhibition also reduced oxidative stress, white matter injury, and brain atrophy and improved functional outcomes. Histologic results were confirmed by MRI. Src kinase phosphorylation and matrix metalloproteinase-9 activity were increased by EP1R activation and decreased by EP1R inhibition. EP1R regulated matrix metalloproteinase-9 activity through Src kinase signaling, which mediated EP1R toxicity after collagenase-induced ICH. We conclude that prostaglandin E_2 EP1R activation plays a toxic role after ICH through mechanisms that involve the Src kinases and the matrix metalloproteinase-9 signaling pathway. EP1R inhibition could be a novel therapeutic strategy to improve outcomes after ICH.

© 2015 Published by Elsevier Inc.

1. Introduction

Spontaneous intracerebral hemorrhage (ICH) is a devastating type of stroke. It causes brain damage through many mechanisms. Hematoma formation and expansion within the brain cause the primary, mechanical damage. Inflammatory cascades, including those mediated by certain prostaglandins, contribute to the progression of secondary injury (Keep et al., 2012; Wang, 2010; Wu et al., 2010), which causes severe neurologic deficits in patients. Interventions are needed that can limit detrimental effects of neuroinflammation on brain function and improve outcomes after ICH.

Prostaglandin E_2 (PGE_2) is predominant in the brain. This bioactive lipid is synthesized from cyclooxygenases and PGE_2 synthases. We and others have reported that the expression of cyclooxygenase-2 and microsomal PGE_2 synthase-1 is increased after ICH (Gong et al., 2001; Wu et al., 2011b). Consequently, PGE_2 accumulates in the perihematomal region after ICH (Chu et al., 2004). Importantly, selective inhibition of cyclooxygenase-2 reduces ICH injury and improves outcomes (Chu et al., 2004). PGE_2 acts through

* Corresponding authors at: Department of Anesthesiology and Critical Care Medicine, Johns Hopkins University, School of Medicine, 720 Rutland Ave, Ross Bldg 370B, Baltimore, MD 21205, USA. Tel.: +1 443 287 5490 (J. Wang). Tel.: +86 133 9123 2009 (T. Wu).
E-mail addresses: twu163@163.com (T. Wu), jwang79@jhmi.edu (J. Wang).
[1] These authors contributed equally to this work.

http://dx.doi.org/10.1016/j.bbi.2015.02.011
0889-1591/© 2015 Published by Elsevier Inc.

UNCORRECTED PROOF

four G-protein-coupled receptor subtypes known as EP1–EP4. These receptors have divergent downstream signaling cascades and functional effects depending on the physiologic or pathologic context (Andreasson, 2010a,b). Deletion or inhibition of the EP1 receptor (EP1R) was shown to reduce ischemic brain injury (Abe et al., 2009; Kawano et al., 2006). Based on these results, PGE_2 signaling might also contribute to inflammation-mediated secondary ICH injury (Wang and Dore, 2007b). However, the role of EP1R in ICH remains to be determined because the pathogenesis of ICH is different from that of ischemic stroke.

Mechanisms that underlie EP1R-mediated neurotoxicity are unknown, but one possibility is the Src pathway (Fukumoto et al., 2010). Two studies have shown that Src kinase activation mediates thrombin-induced blood–brain barrier disruption (Liu et al., 2010) and that inhibition of Src kinase activity reduces blood toxicity (Ardizzone et al., 2007). Matrix metalloproteinase (MMP)-9 mediates neuroinflammation and has been implicated in ICH pathology (Wang and Tsirka, 2005a; Xue et al., 2009b). Although Src kinases could phosphorylate and regulate MMP-9 (Liu and Sharp, 2011), a direct link between the two has not been established.

In the present study, we investigated the role of EP1R after ICH and its mechanism of action. We hypothesized that EP1R activation aggravates ICH injury but that its blockade reduces injury through the Src kinases and the MMP-9 signaling pathway. To test this hypothesis, we examined the effects of selective EP1R agonist ONO-DI-004 (DI-004) and antagonist SC51089 (Abe et al., 2009; Jones et al., 2009; Kawano et al., 2006) on ICH outcomes in mice. We also measured inflammatory cells, reactive oxygen species (ROS) production, and Src kinase and MMP activity in the hemorrhagic brain. The role of Src kinases in EP1R-mediated ICH injury was confirmed by using the nonspecific Src family kinase inhibitor PP2. We conclude that EP1R activation elicits toxicity through the Src kinase and MMP-9 signaling pathways after ICH, and that inhibition of EP1R could be used therapeutically to protect against secondary brain injury after ICH.

2. Materials and methods

2.1. Animals

All experimental procedures were conducted in accordance with guidelines of the National Institutes for Health and were approved by the Institutional Animal Care and Use Committee at Johns Hopkins University School of Medicine. Middle-aged C57BL/6 mice (male and female, 10–12 months old, 26–36 g) and aged C57BL/6 mice (male, 18–20 months old, 28–36 g) obtained from Charles River Laboratories (Frederick, MD) were used to enhance the clinical relevance of the study, as ICH occurs more often in middle-aged and elderly people. $Cx3cr1^{GFP/+}$ mice on C57BL/6 background (male, 6 months old, 26–28 g) obtained from Dr. Jonathan Bromberg (University of Maryland, Baltimore, MD) were used to visualize microglia. All efforts were made to minimize the numbers of animals used and ensure minimal suffering.

2.2. Intracerebral hemorrhage models

As we have previously reported (Chang et al., 2014; Wang et al., 2008, 2003), ICH was induced by injecting collagenase VII-S (sterile-filtered, relatively endotoxin-free, 0.075 U in 0.5 μL sterile saline, Sigma, St. Louis, MO), autologous arterial blood (10 μL collected from the central tail artery), or thrombin (from bovine plasma, endotoxin-free, 5 U in 0.2 μL sterile saline, Sigma) into mouse left striatuml at the following stereotactic coordinates: 0.8 mm anterior and 2.0 mm lateral of the bregma, 3.0 mm in depth for collagenase or thrombin injection (over 5 min). In the blood model, autologous whole blood (10 μL) was collected slowly from the central tail artery into a sterile, 10-μL, Hamilton syringe without anticoagulant. A 26-gauge needle was inserted to 3.0 mm below the surface of the skull, and 4 μL of blood was infused over 20 min. The needle was then advanced 0.8 mm ventrally, and after a 6-min pause, the remaining 6 μL of blood was infused over 30 min. The needle was withdrawn slowly (at a rate of 1 mm/min) 10 min after the injection of collagenase, blood, or thrombin to minimize backflow of the infused substance along the needle track. In the three ICH models, the burr hole was sealed with bone wax, and mice were allowed to recover under observation. Rectal temperature of the animals was maintained at 37.0 ± 0.5 °C throughout the experimental and recovery periods.

2.3. Experimental groups

Four experiments were conducted in C57BL/6 mice (middle-aged male, middle-aged female, and aged male) and $Cx3cr1^{GFP/+}$ mice subjected to one of three ICH models. Except where stated otherwise, ICH was induced by collagenase in this study. A schematic diagram of the experimental groups is shown in Supplementary Fig. 1. Sham-operated mice were subjected to needle insertion only. Investigators blinded to the treatment groups evaluated outcomes in all mice and performed calculations and analyses. All mice were included ($n = 537$), but those that died before the end of the study ($n = 51$) were excluded from the final analysis (Supplementary Table 1).

2.3.1. Experiment 1

Middle-aged C57BL/6 male mice were subjected to collagenase-induced ICH and randomly assigned to receive EP1R antagonist SC51089 (Ki values: 0.8 μM for EP1R and >10 μM for EP2–4 receptors; Biomol, Plymouth Meeting, PA), EP1R agonist DI-004 (Ki values: 150 nM for EP1R and >10 μM for the other receptors; ONO Pharmaceutical Co., Ltd., Tokyo, Japan), or vehicle by using the website Randomization.com (http://www.randomization.com) (Chang et al., 2014). The selectivity of SC51089 and DI-004 for EP1R has been established (Ahmad et al., 2006; Jones et al., 2009; Kawano et al., 2006). SC51089 (5, 10, 20 μg/kg) or vehicle (ddH_2O) was administered intraperitoneally (i.p.) at 2 h and 6 h after ICH and then twice daily for up to 3 days. DI-004 (0.2 μL, 10 nM) or vehicle (0.5% dimethyl sulfoxide [DMSO] in ddH_2O) was injected into the left striatum immediately after collagenase injection at the same stereotactic coordinates (0.8 mm anterior, 3.0 mm ventral, and 2.0 mm lateral to bregma). We chose the delivery route, dosing, and treatment regimens for SC51089 and DI-004 based on previous work and our pilot studies (Abe et al., 2009; Ahmad et al., 2006; Kawano et al., 2006). Endpoints included lesion volume, brain water content, neurologic deficits, and cell and neuronal death (72 h); striatum volume and white matter injury (day 28); Western blots, gelatin gel zymography, *in situ* zymography, and brain tissue hemoglobin content (24 h); and markers for oxidative damage (24 h) and cellular inflammation (ionized calcium-binding adapter molecule 1 [Iba1], glial fibrillary acidic protein [GFAP], and myeloperoxidase [MPO]; 72 h). A subgroup of middle-aged C57BL/6 male mice and mature adult $Cx3cr1^{GFP/+}$ mice were subjected to collagenase-induced ICH and then examined for EP1R expression and cellular localization (72 h).

2.3.2. Experiment 2

SC51089 (10 μg/kg) or vehicle (ddH_2O) was administered i.p. to randomly assigned middle-aged C57BL/6 male mice at 2 h and 6 h after collagenase-induced ICH and then twice daily for 3 days. MRI was performed on days 3 and 28 to assess lesion volume and on day 28 to assess brain atrophy and white matter injury.

UNCORRECTED PROOF

Please cite this article in press as: Zhao, X., et al. Toxic role of prostaglandin E_2 receptor EP1 after intracerebral hemorrhage in mice. Brain Behav. Immun. (2015), http://dx.doi.org/10.1016/j.bbi.2015.02.011

2.3.3. Experiment 3

Middle-aged C57BL/6 male mice were subjected to collagenase-induced ICH and then randomly assigned to receive EP1R agonist DI-004, DI-004 plus 2.0 mg/kg Src kinase inhibitor PP2 (4-amino-5-(4 chlorophenyl)-7-(t-butyl) pyrazolo [3,4-D] pyrimidine, Cayman Chemical, Ann Arbor, MI), or vehicle (saline). DI-004 was administered as in Experiment 1. PP2 was administered i.p. 2 h after DI-004 injection and then once daily for up to 3 days (Liu et al., 2008). Endpoints included Western blotting, gel and *in situ* zymography (24 h), lesion volume, brain edema, neurologic deficits, and cell and neuronal death (72 h). One group of mice was randomly assigned to receive SC51089 (10 μg/kg, i.p.), PP2 (2.0 mg/kg, i.p.), SC51089 (10 μg/kg, i.p.) plus PP2 (2.0 mg/kg, i.p.), or vehicle (saline). SC51089 was administered as in Experiment 2. In SC51089-treated and -untreated groups, PP2 or vehicle was given immediately after SC51089 injection and then once daily for up to 3 days. Assessments included brain water content and neurologic deficits (72 h).

2.3.4. Experiment 4

Middle-aged C57BL/6 male mice were subjected to ICH induced by blood or thrombin and then randomly assigned to receive SC51089 (10 μg/kg) or vehicle (ddH_2O), as described in Experiment 2. Assessments included gel zymography (24 h), brain water content, and neurologic deficits (72 h). To determine the therapeutic window of the SC51089 treatment, we subjected middle-aged male mice to the collagenase-induced ICH model and randomly assigned them to receive SC51089 (10 μg/kg) or vehicle starting at 6, 12, 18, or 24 h after ICH. Lesion volume and neurologic deficits were examined at 72 h. To determine whether the protection is present in female and aged mice, we subjected middle-aged female mice and aged male mice to collagenase-induced ICH and then randomly assigned them to receive SC51089 (10 μg/kg) or vehicle, as described in Experiment 2. Lesion volume and neurologic deficits were examined at 72 h.

2.4. Tissue processing and histology

Mice were deeply anesthetized with isoflurane and euthanized at various time points after ICH by transcardial perfusion with phosphate-buffered saline (PBS) followed by 4% paraformaldehyde. Brains were removed, kept in 4% paraformaldehyde overnight, and then transferred to 30% sucrose in PBS. Coronal sections were cut on a cryostat from the level of the olfactory bulbs to the visual cortex. Based on our established protocol of brain tissue processing and histology (Chang et al., 2014), we used coronal sections through the entire striatum for Luxol fast blue/Cresyl violet staining, Fluoro-Jade B (FJB) staining, propidium iodide (PI) staining, hydroethidine analysis, and gelatin *in situ* zymography (Chang et al., 2014). Luxol fast blue/Cresyl violet staining was used to measure brain lesion volume (Wu et al., 2012), FJB staining was used to quantify degenerating neurons (Wang and Tsirka, 2005b), *in vivo* PI labeling was used to detect cell death (Chang et al., 2014; Zhu et al., 2012), and *in situ* detection of oxidized hydroethidine was used to measure superoxide production (Wu et al., 2012). Mice assigned to PI staining (day 3, $n = 6$/group), hydroethidine analysis (day 1, $n = 6$/group), and gelatin *in situ* zymography were perfused with PBS only. The brains were frozen rapidly in dry ice, stored at −80 °C, and then cut into 30-μm sections on a cryostat.

2.5. Neurologic function evaluations

Neurologic deficits were assessed by a 24-point scoring system, the wire-hanging test, and/or the corner turn test on days 1, 3, and 28 post-ICH (Abe et al., 2009; Wang et al., 2006; Zhu et al., 2014). In the neurologic deficit scoring system, we evaluated mice in six neurologic tests, including body symmetry, gait, climbing, circling behavior, front limb symmetry, and compulsory circling. Each test was graded from 0 to 4, establishing a maximum deficit score of 24 (Wu et al., 2012). We evaluated grip strength, balance, and endurance by using the wire-hanging test (Zhu et al., 2014), in which a mouse must suspend its body by its forelimbs on an iron wire stretched between two posts (55 cm long suspended horizontally, 50 cm above the ground). Adhesive tape prevented mice from gripping with their hind limbs, and a pillow prevented injury from falls. The time that the mouse was able to remain suspended was recorded. In the corner turn test (Chang et al., 2014), we corralled the mouse into a 30° corner and recorded which direction it turned to exit. The percentage of left turns was calculated.

2.6. Brain lesion volume

On day 3 after collagenase-induced ICH, mice underwent neurologic evaluation and then were euthanized. Coronal sections were stained with Luxol fast blue (for myelin) and Cresyl violet (for neurons) at 10 rostral–caudal levels that were spaced 360 μm apart. The unstained area indicated the injured territory in the brain sections. The lesion volume in cubic millimeters was calculated by summing the damaged areas of each section and multiplying by the interslice distance, as previously described (Chang et al., 2014; Wu et al., 2012).

2.7. Brain water content

At 72 h after ICH induced by collagenase, blood, or thrombin ($n = 6$/group), we determined brain edema by calculating brain water content as follows: (wet weight − dry weight)/wet weight × 100% (Wu et al., 2012).

2.8. Spectrophotometric assay for brain tissue hemoglobin

The hemoglobin content in the striatal tissue of brains was quantified with Drabkin's reagent (Sigma; $n = 10$/group) at 24 h after collagenase injection, as described previously (Chang et al., 2014; Wang et al., 2003). According to our previous work, collagenase-induced hematoma reaches its maximum size at 5–6 h (Chang et al., 2011; Wang and Dore, 2007a).

2.9. Magnetic resonance imaging

In vivo MRI experiments were performed on a horizontal 11.7 Tesla MR scanner (Bruker Biospin, Billerica, MA, USA) equipped with triple-axis gradient (maximum gradient strength = 74 Gauss/cm) using a volume excitation coil and a 4-channel phased array mouse head receive-only coil. Animals were anesthetized with 1–1.5% isoflurane in a mix of oxygen and air at a 1:3 ratio and placed in an animal holder (Bruker Biospin). Respiration was monitored with a pressure sensor (SAII, Stony Brook, NY, USA) and maintained at 50–60 breaths per minute by adjusting the concentration of isoflurane. Multi-slice T2-weighted images were collected by using a rapid acquisition with refocused echoes (RARE) sequence with the following parameters: echo time/repetition time = 60/3800 ms, RARE-factor = 8, four signal averages, field of view = 15 mm × 15 mm, 28 slices with 0.5 mm slice thickness, in-plane resolution of 0.08 mm × 0.08 mm, and an imaging time of 12 min. Multi-slice *in vivo* diffusion tensor imaging (DTI) was performed by using a four-segment diffusion-weighted echo-planar imaging sequence with the following parameters: echo

UNCORRECTED PROOF

Please cite this article in press as: Zhao, X., et al. Toxic role of prostaglandin E_2 receptor EP1 after intracerebral hemorrhage in mice. Brain Behav. Immun. (2015), http://dx.doi.org/10.1016/j.bbi.2015.02.011

time/repetition time = 24/14000 ms; one signal average; 30 diffusion directions; $b = 1500$ s/mm^2; an in-plane resolution of 0.12 mm × 0.12 mm with a partial Fourier factor of 1.4 in the phase-encoding direction, and the same field of view, slice thickness, and number of slices as the T2-weighted images. With respiratory gating, the total imaging time was approximately 30 min. All animals recovered in 5 min after imaging. We reconstructed the diffusion tensor at each pixel along with apparent diffusion coefficient and fractional anisotropy using the log-linear fitting method implemented in DTIStudio (http://www.mristudio.org). In mice that had undergone collagenase-induced ICH, we manually defined the hematoma volume on day 3 and residual lesion volume and striatal volume on day 28 in the T2-weighted images using ROIEditor (http://www.mristudio.org). White matter injury on day 28 post-ICH was analyzed from DTI. We manually defined the ipsilateral corpus callosum from the midline to the lateral edge of the lateral ventricles in the fractional anisotropy images using ROIEditor and obtained the average fractional anisotropy value in the region for each subject.

2.10. Immunofluorescence

Immunofluorescence was carried out as described previously (Wang and Tsirka, 2005a). The primary antibodies used were rabbit anti-Iba1 (microglia marker; 1:500; Wako Chemicals, Richmond, VA); rat anti-GFAP (astrocyte marker; 1:250; Life Technologies, Grand Island, NY); rabbit anti-MPO (neutrophil marker; 1:500; Dako, Carpinteria, CA); rabbit anti-degraded myelin basic protein (dMBP, labels degraded myelin; 1:2000; Millipore, Billerica, MA); rabbit anti-amyloid precursor protein (APP, labels damaged axons; 1:200; Sigma); rabbit anti-EP1R (1:100; Cayman Chemical); mouse anti-NeuN (neuronal marker; 1:1000; Millipore, Billerica, MA); and rat anti-CD11b (microglia and myeloid cell marker; 1:100; AbD Serotec, Raleigh, NC). Free-floating sections were then incubated with secondary antibodies conjugated to Alexa Fluor 488 (1:1000; Molecular Probes, Eugene, OR) and/or Cy3 (1:1000; Jackson Labs, West Grove, PA). Stained sections were examined with a Nikon Eclipse 90i fluorescence microscope (Nikon, Tokyo, Japan). Control sections were processed as above,

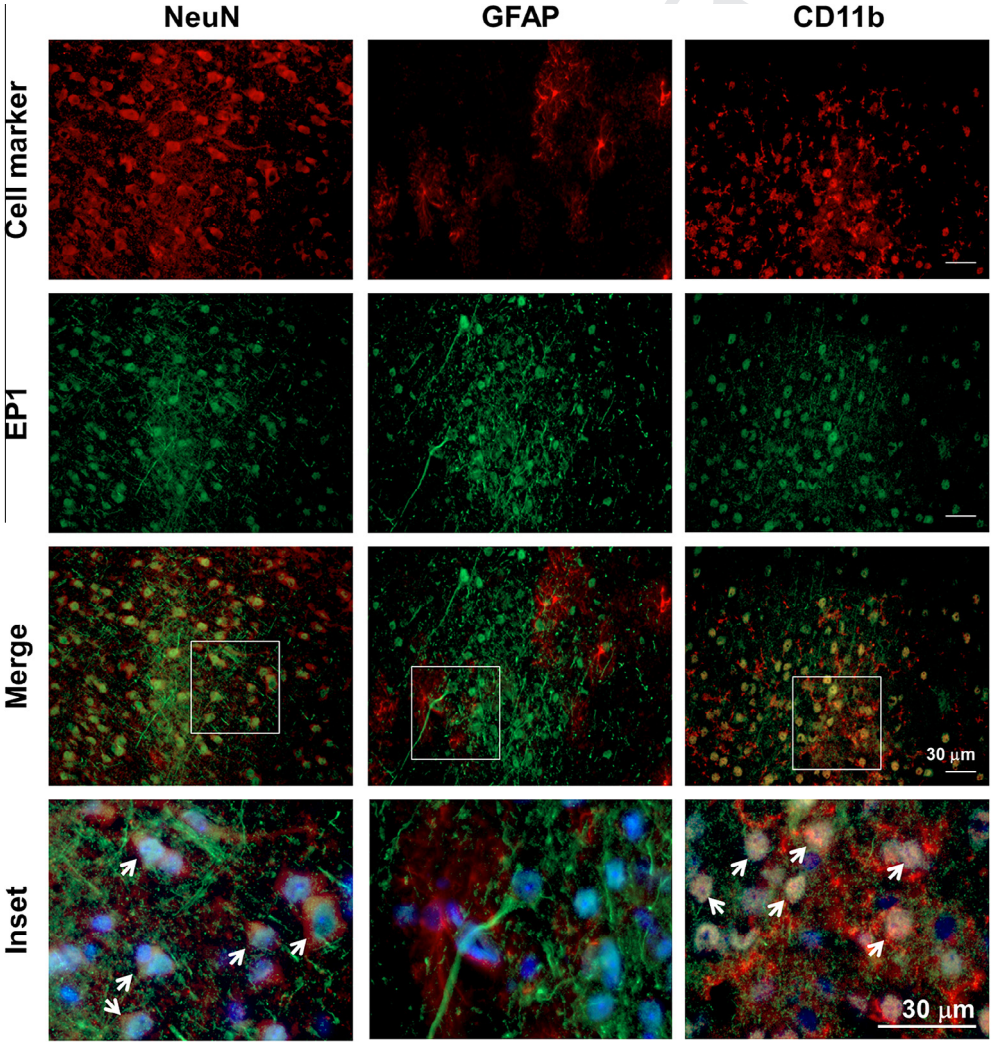

Fig. 1. Identification of EP1R–positive cells in the perihematomal region by double immunofluorescence labeling on day 3 after collagenase-induced ICH. EP1R immunoreactivity is shown in green, and immunolabeling of NeuN (neurons), GFAP (astrocytes), or CD11b (microglia and myeloid cells) is shown in red. EP1R immunoreactivity colocalized primarily with NeuN$^+$ neurons and their axons and, to a lesser extent, with CD11b$^+$ cells, but not with GFAP$^+$ astrocytes. CD11b$^+$ cells with EP1R immunoreactivity were round and lacked processes. CD11b$^+$ cells without EP1R immunoreactivity were typical process-bearing microglia. Insets represent higher magnification of the boxed areas in the corresponding merged images. Sections were stained with DAPI (blue) to label nuclei. Arrows indicate the colocalization of EP1R and CD11b. Three sections were analyzed per animal. Scale bars: 30 μm, $n = 3$ mice. (For interpretation of the references to color in this figure legend, the reader is referred to the web version of this article.)

Please cite this article in press as: Zhao, X., et al. Toxic role of prostaglandin E_2 receptor EP1 after intracerebral hemorrhage in mice. Brain Behav. Immun. (2015), http://dx.doi.org/10.1016/j.bbi.2015.02.011

except that primary antibodies were omitted. The specificity of the EP1R antibody was confirmed by preincubation of the antibody with EP1R blocking peptide (Tober et al., 2006).

2.11. Western blotting

A 4-mm coronal section containing the striatum was collected at 24 h after collagenase-induced ICH, as described previously (Chang et al., 2014). Twenty-microgram protein samples were separated by 4–12% SDS–PAGE and transferred onto polyvinylidene difluoride membranes. The membranes were blocked and probed with the following primary antibodies: rabbit anti-cleaved caspase-3 (1:1000; Cell Signaling, Danvers, MA), rabbit anti-caspase-3 (1:1000; Cell Signaling), mouse anti-nitrotyrosine (1:40,000; Millipore), rabbit anti-Src (1:1000; Cell Signaling), rabbit anti-phospho-Src (Tyr416, 1:1000; Cell Signaling), and β-actin (1:5000; Santa Cruz Biotechnology, Santa Cruz, CA). Resulting protein bands were scanned and analyzed with ImageJ software (version 1.42q, NIH). Optical density values were normalized to the corresponding loading control intensity on each gel and were expressed as fold change over values from sham-operated mice.

2.12. Protein oxidation assay

Protein carbonylation was determined at 24 h after collagenase-induced ICH with an OxyBlot protein oxidation detection kit (Millipore) for protein carbonyl groups, as previously described (Chang et al., 2014).

2.13. Gelatin in situ and gel zymography

Both zymography protocols were performed as previously described (Chang et al., 2014; Wang and Tsirka, 2005a).l *In situ* gelatinolytic activity was detected on freshly frozen, 20-μm-thick unfixed brain sections by using an EnzChek Gelatinase Assay kit (Life Technologies) at 72 h after collagenase-induced ICH ($n = 5$/group). Cleavage of DQ gelatin by MMP-2 or MMP-9 results in a green fluorescent product (excitation/emission: 495/515 nm). For gelatin gel zymography, protein samples were prepared from mouse brains containing the striatum (Chang et al., 2014) at 72 h after collagenase-induced ICH or 24 h after thrombin-induced ICH ($n = 6$/group). Equal amounts of protein (500 μg) were purified with gelatin-Sepharose 4B (GE Healthcare Bio-Sciences,

PROOF

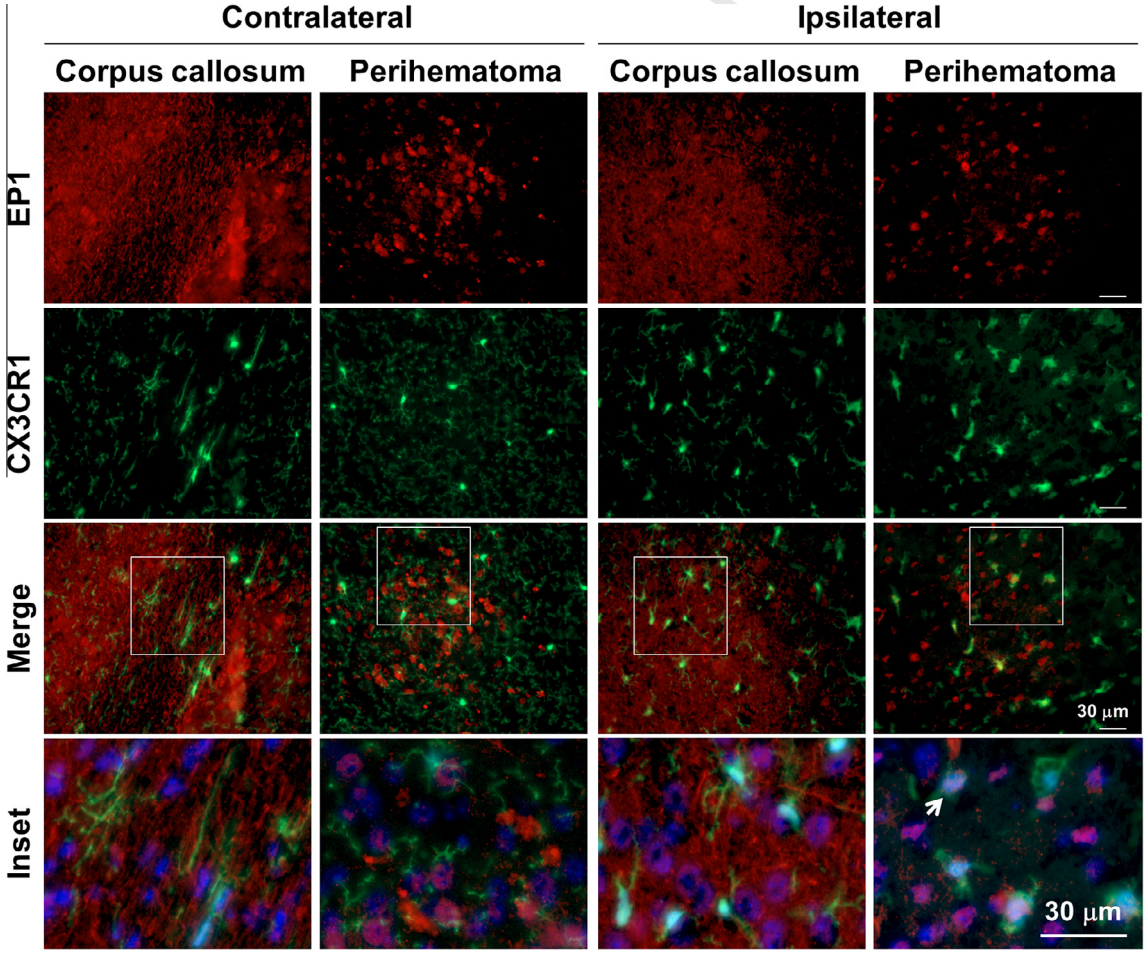

Fig. 2. Colocalization of EP1R and microglia in the corpus callosum and perihematomal region on day 3 after collagenase-induced ICH in Cx3cr1$^{GFP/+}$ mice. EP1R immunoreactivity is shown in red, and Cx3cr1^{+} microglia are green. In the ICH brain, EP1R immunoreactivity can be clearly seen in fiber tracts of the contralateral corpus callosum and in neuron-like cells in the ipsilateral and contralateral striatum. However, no colocalization is present in resting or reactive process-bearing Cx3cr1^{+} microglia in the ipsilateral or contralateral corpus callosum and striatum. Insets represent higher magnification of the boxed areas in the corresponding merged images. Sections were stained with DAPI (blue) to label nuclei. The arrow indicates colocalization of EP1R and CX3CR1. Three sections were analyzed per animal. Scale bars: 30 μm, $n = 5$ mice. (For interpretation of the references to color in this figure legend, the reader is referred to the web version of this article.)

Please cite this article in press as: Zhao, X., et al. Toxic role of prostaglandin E_2 receptor EP1 after intracerebral hemorrhage in mice. Brain Behav. Immun. (2015), http://dx.doi.org/10.1016/j.bbi.2015.02.011

Piscataway, NJ) and separated on a 10% Tris–glycine gel with 0.1% gelatin as substrate. A mixture of mouse pro-MMP-9 (98 kDa) and pro-MMP-2 (72 KDa) (R&D Systems, Minneapolis, MN) was used as the gelatinase standard. Gels were analyzed densitometrically (ImageJ) on coded samples. MMP-2/9 activity was measured by optical density and quantified as fold increase over values from sham controls.

2.14. Quantification of immunofluorescence, PI, FJB, hydroethidine, Luxol fast blue staining, and in situ gelatinolytic activity

Immunofluorescence, PI, FJB, hydroethidine, Luxol fast blue staining, and *in situ* gelatinolytic activity were quantified on stained sections at 1.10, 0.74, and −0.10 mm from the bregma. The region of interest was defined in the striatum within one

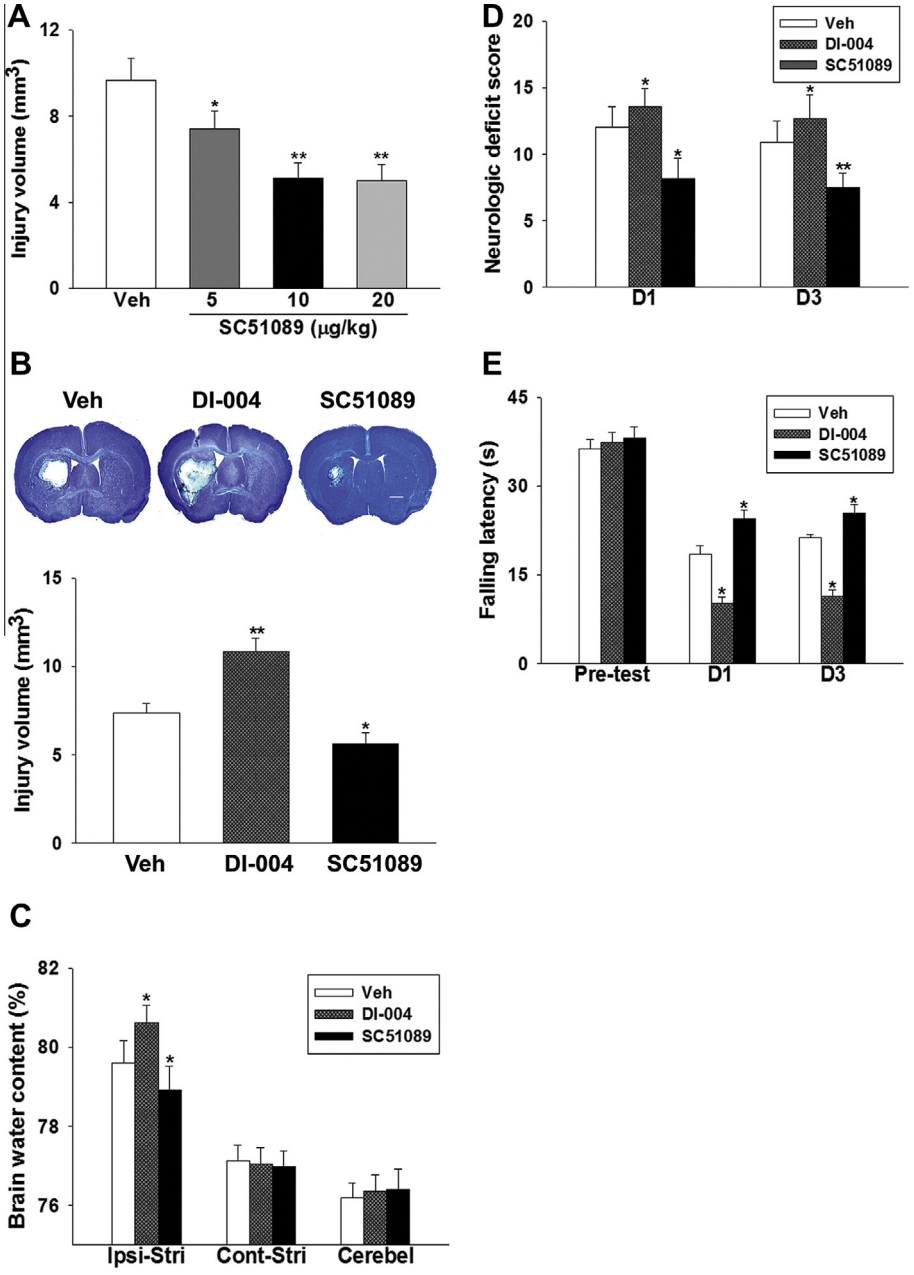

Fig. 3. Effect of EP1R activation or inhibition on brain injury volume, brain edema, and neurologic function in middle-aged male mice subjected to collagenase-induced ICH. (A) Bar graph shows reduction of brain injury volume on day 3 post-ICH in mice administered EP1R antagonist SC51089 intraperitoneally at 2 h and 6 h after ICH and then twice daily for up to 3 days (n = 6 mice/group). (B) Representative Luxol fast blue/Cresyl violet-stained brain sections on day 3 post-ICH; injured areas lack staining and are circled in black. Quantification analysis shows that intrastriatal administration of EP1R agonist DI-004 immediately after ICH exacerbated brain injury volume, whereas EP1R inhibition by SC51089 reduced brain injury volume (n = 6 mice/group) compared to that in vehicle (Veh)-treated ICH mice. Scale bar: 2 mm. (C) On day 3 post-ICH, mice that had received DI-004 exhibited increased brain water content, whereas those that had received SC51089 exhibited reduced brain water content, compared to levels in vehicle-treated ICH mice (n = 8 mice/group). (D and E) Compared to vehicle-treated mice, DI-004-treated mice had more severe neurologic deficit (D) and shorter falling latency in the wire-hanging test (E), whereas SC51089-treated mice had improved neurologic function and increased falling latency on days 1 (D1) and 3 (D3) post-ICH (n = 12 mice/group). In A–E, the vehicle used was ddH_2O. We omitted the vehicle group for DI-004 (0.5% DMSO) because it did not affect lesion volume, brain edema, or neurologic deficits differently than ddH_2O did. Values are mean ± SD; $^{*}p < 0.05$; $^{**}p < 0.01$ vs. vehicle group. Ipsi-Stri, ipsilateral striatum; Cont-Stri, contralateral striatum; Cerebel, cerebellum. (For interpretation of the references to color in this figure legend, the reader is referred to the web version of this article.)

Please cite this article in press as: Zhao, X., et al. Toxic role of prostaglandin E_2 receptor EP1 after intracerebral hemorrhage in mice. Brain Behav. Immun. (2015), http://dx.doi.org/10.1016/j.bbi.2015.02.011

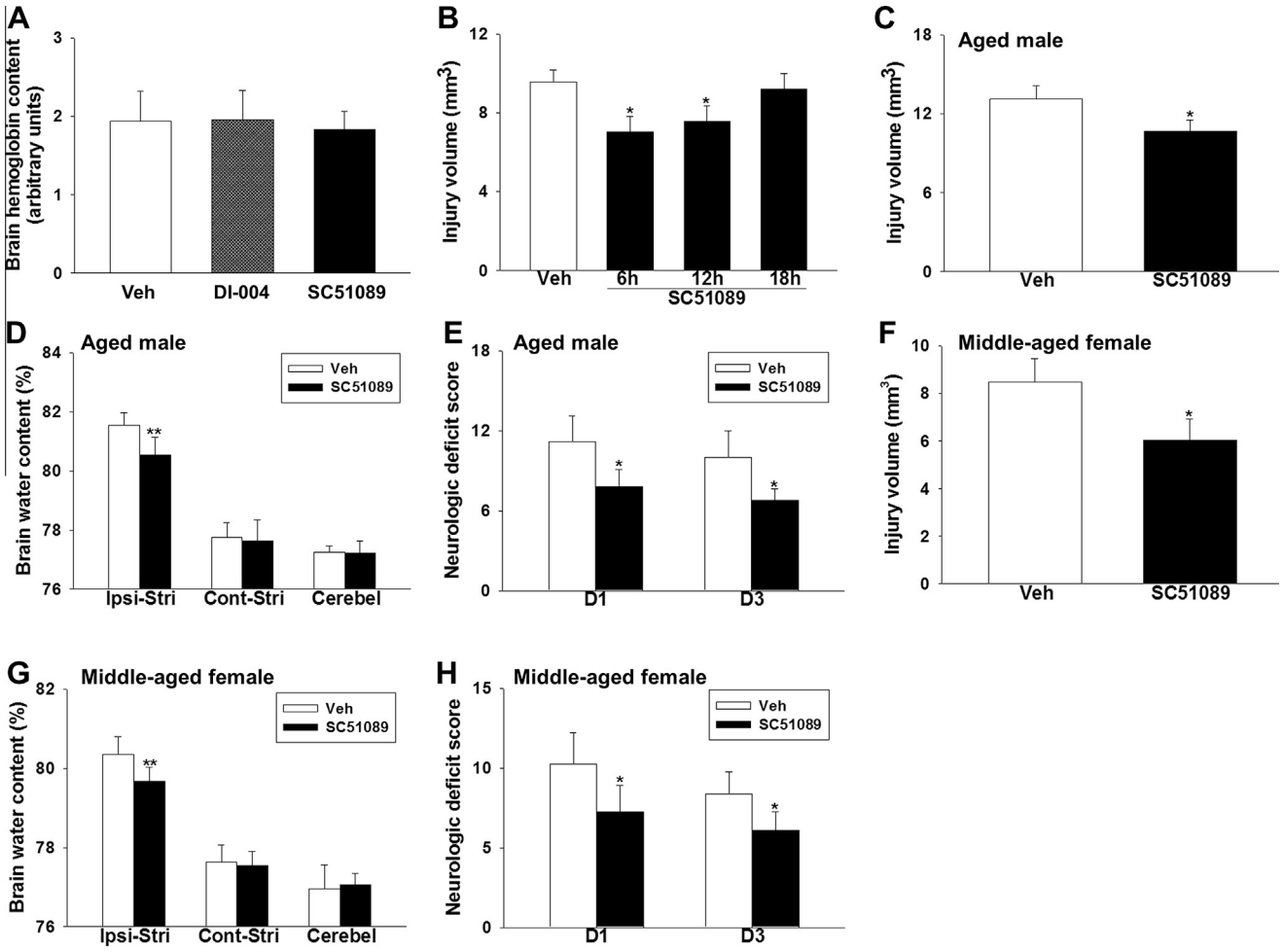

Fig. 4. Effect of EP1R activation and inhibition on collagenase-induced bleeding in middle-aged male mice and effect of EP1R inhibition on outcomes in middle-aged female and aged male mice. (A) Hemoglobin levels in the striatum did not differ between DI-004-, SC51089-, and vehicle (Veh)-treated mice on day 1 after ICH, $n = 6$ mice/group. (B) The therapeutic window of SC51089 treatment after collagenase-induced ICH in middle-aged male mice. SC51089 treatment significantly reduced brain injury volume on day 3 post-ICH when administered up to 12 h after ICH, $n = 6$ mice/group. (C–E) SC51089 treatment is neuroprotective in aged male mice. On day 3 after collagenase-induced ICH, brain injury volume (C), brain water content (D), and neurologic deficit score (E) were lower in aged male mice treated with SC51089 than in those treated with vehicle, $n = 5$ mice/group. (F–H) SC51089 treatment is neuroprotective in middle-aged female mice. On day 3 after middle-aged female mice were subjected to collagenase-induced ICH, brain injury volume (F), brain water content (G), and neurologic deficit score (H) were lower in the SC51089-treated group than in the vehicle-treated group, $n = 6$–8 mice/group. Values are mean ± SD; $^{*}p < 0.05$; $^{**}p < 0.01$ vs. vehicle group. Ipsi-Stri, ipsilateral striatum; Cont-Stri, contralateral striatum; Cerebel, cerebellum.

20× field that corresponded to an area ~460 μm from the lateral edge of the hematoma along the rostral–caudal axis. In each animal, we examined four randomly selected fields at 200× magnification in three sections with similar hematoma sizes (Supplementary Fig. 2). Quantifications from 12 locations were averaged and expressed as positive cells (Iba1-, GFAP-, MPO-, PI-, FJB-, and *in situ* gelatinolytic-positive cells), positive areas (dMBP-labeled degraded myelin and Luxol fast blue-stained intact myelin tract), or fluorescence intensity (APP-labeled damaged axons and oxidized hydroethidine) per cubic millimeter.

2.15. Primary neuronal culture

Corticostriatal neurons were prepared from embryos at gestational day 15.5 and cultured in serum-free conditions as previously described (Chang et al., 2011, 2014; Wang et al., 2006). The tissue was dissociated in Hibernate-A medium (containing B27 supplement), and papain digestion was used to obtain single cells. The cells were seeded onto poly-D-lysine–coated plates at a density of 5×10^4 cells/cm^2. They were maintained in Neurobasal medium with B27 supplement and were used at 7 days *in vitro*. The corticostriatal cultures contained mostly neurons and <2% glial cells.

2.16. Lactate dehydrogenase assay

Cell viability was determined by lactate dehydrogenase release into cell culture medium (Chang et al., 2014). Neurons were grown in 24-well plates for 24 h after treatment with or without hemoglobin (5 μM in sterile water) and SC51089 (10 μM in sterile water). Three wells were used for each condition in each experiment. Experiments were repeated three times with different batches of cells.

2.17. Statistics

All data are presented as mean ± standard deviation. Differences between two groups were determined by two-tailed Student's *t*-test. The statistical comparisons among multiple groups were made by using one-way or two-way ANOVA followed by Bonferroni correction. Mortality rates were compared between groups by chi-square test. Statistical significance was set at $p < 0.05$.

UNCORRECTED PROOF

Please cite this article in press as: Zhao, X., et al. Toxic role of prostaglandin E_2 receptor EP1 after intracerebral hemorrhage in mice. Brain Behav. Immun. (2015), http://dx.doi.org/10.1016/j.bbi.2015.02.011

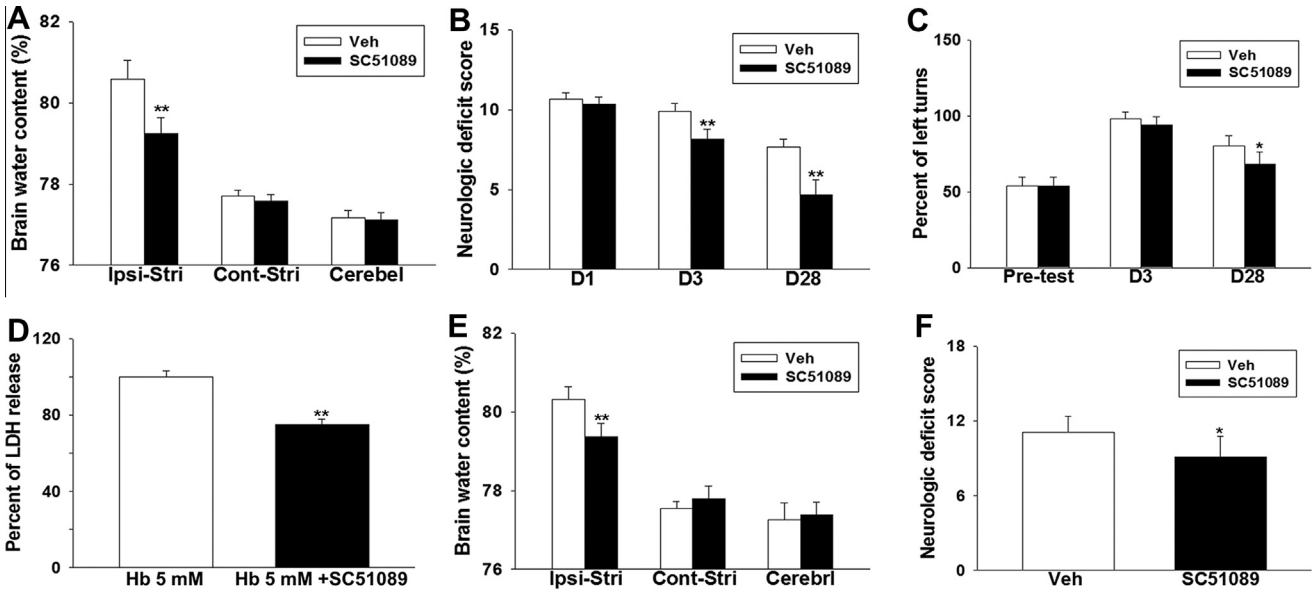

Fig. 5. Effect of EP1R inhibition by SC51089 on outcomes of blood- and thrombin-induced ICH in middle-aged male mice. In the blood ICH model, SC51089 treatment reduced brain water content on day 3 (A), neurologic deficit score on days 3 and 28 (B), and corner turn test performance on day 28 post-ICH (C), compared with values in the vehicle (Veh) group, $n = 8–12$ mice/group. (D) SC51089 treatment decreased neuronal vulnerability to hemoglobin-induced toxicity. Exposure of primary neurons to hemoglobin (Hb, 5 mM) for 24 h caused a significant increase in lactate dehydrogenase (LDH) release. Concurrent treatment of neurons with SC51089 (10 μM) reduced Hb-induced LDH release, $n = 3$ per group. In the thrombin-induced ICH model, SC51089 treatment reduced brain water content (E) and neurologic deficit score (F) on day 1, compared with values in the vehicle group, $n = 8–12$ mice/group. Values are mean ± SD; $^{*}p < 0.05$; $^{**}p < 0.01$ vs. vehicle group. Ipsi-Stri, ipsilateral striatum; Cont-Stri, contralateral striatum; Cerebel, cerebellum.

3. Results

3.1. EP1R is expressed in neurons but not in Cx3cr1^{+} microglia after ICH induced by collagenase

To clarify the cell type that expresses EP1R on day 3 after ICH, we performed double-immunolabeling with cell-type–specific antibodies. In the contralateral striatum, EP1R was present in NeuN^{+} neurons. In the ipsilateral striatum, EP1R colocalized primarily with NeuN^{+} neurons and their axons and, to a lesser extent, with CD11b^{+} cells, but not with GFAP^{+} astrocytes; CD11b^{+} cells with EP1R immunoreactivity were round and lacked processes. CD11b^{+} cells without EP1R immunoreactivity were typical process-bearing microglia ($n = 3$; Fig. 1). To further confirm whether EP1R was present in CD11b^{+} microglia, we stained for EP1R in brain sections from Cx3cr1$^{GFP/+}$ mice subjected to ICH. EP1R was expressed in the fiber tracts of ipsilateral and contralateral corpus callosum and was present in neuron-like cells in the ipsilateral and contralateral striatum. However, it was not present in resting or reactive, process-bearing Cx3cr1^{+} microglia in the corpus callosum or striatum ($n = 5$; Fig. 2).

3.2. EP1R inhibition mitigates whereas EP1R activation exacerbates brain injury, brain edema, and neurobehavioral deficits after collagenase-induced ICH

To understand the role of EP1R after ICH, we administered EP1R antagonist SC51089 i.p. and agonist DI-004 intrastriatally to middle-aged male mice that had undergone collagenase-induced ICH. We first determined the optimal dose of SC51089 when given at 2 h and 6 h after ICH and then twice daily for up to 3 days. A reduction in injury volume was observed at 5 μg/kg (−23%; $p < 0.05$; $n = 6$ mice/group) and was greatest at 10 μg/kg (−47%; $F = 36.76$, $p < 0.01$; $n = 6$ mice/group; Fig. 3A). Because the reduction in injury volume at 20 μg/kg did not differ from that at 10 μg/kg ($p > 0.05$; $n = 6$ mice/group; Fig. 3A), we used 10 μg/kg of SC51089 in subsequent studies. The mortality rate was lower in the SC51089-treated group (3.3%, 4 of 122) than in the vehicle-treated group (10.8%, 16 of 148, $p < 0.05$, Supplementary Table 1). We further confirmed that, compared with outcomes in the vehicle group, EP1R activation by DI-004 worsened brain injury volume ($F = 104.79$, $p < 0.01$; $n = 6$ mice/group; Fig. 3B) and increased brain water content on day 3 post-ICH ($F = 22.66$, $p < 0.01$; $n = 8$ mice/group; Fig. 3C). These indicators of injury were associated with worse neurologic function, as measured by neurologic deficit score ($F = 42.32$, $p < 0.05$ on day 1; $F = 36.66$, $p < 0.05$ on day 3; $n = 12$ mice/group; Fig. 3D) and falling latency in the wire-hanging test ($F = 346.08$, $p < 0.05$ on day 1; $F = 343.23$, $p < 0.05$ on day 3; $n = 12$ mice/group; Fig. 3E). In contrast, EP1R inhibition with SC51089 reduced brain injury volume (from 7.4 ± 0.6 mm^3 to 5.6 ± 0.6 mm^3) and brain water content and improved neurologic deficit score and falling latency compared with the corresponding values in the vehicle-treated group (all $p < 0.05$; $n = 6–12$ mice/group; Fig. 3B–E). We omitted the vehicle group for DI-004 (0.5% DMSO) in Fig. 3B–E because the outcomes were no different from those of the vehicle group for SC51089 (ddH_2O) for lesion volume, brain edema, and neurologic deficits (Supplementary Fig. 3).

To ascertain whether EP1R activation or inhibition affects collagenase-induced bleeding volume, we measured hemoglobin content in the striatum at 24 h after collagenase injection, when hematoma reaches its maximum in this model (Chang et al., 2011; Wang and Dore, 2007a). No significant difference was observed between vehicle-treated and DI-004- or SC51089-treated mice ($F = 0.25$, both $p > 0.05$; $n = 6$ mice/group; Fig. 4A).

We further determined the therapeutic window of SC51089 treatment after collagenase-induced ICH in middle-aged male mice. Reduction in injury volume was observed when SC51089 was administered 6 h or 12 h after ICH ($F = 16.40$, both $p < 0.05$; $n = 6$ mice/group), but not when the administration was delayed by 18 h ($p > 0.05$; $n = 6$ mice/group; Fig. 4B).

UNCORRECTED

Please cite this article in press as: Zhao, X., et al. Toxic role of prostaglandin E_2 receptor EP1 after intracerebral hemorrhage in mice. Brain Behav. Immun. (2015), http://dx.doi.org/10.1016/j.bbi.2015.02.011

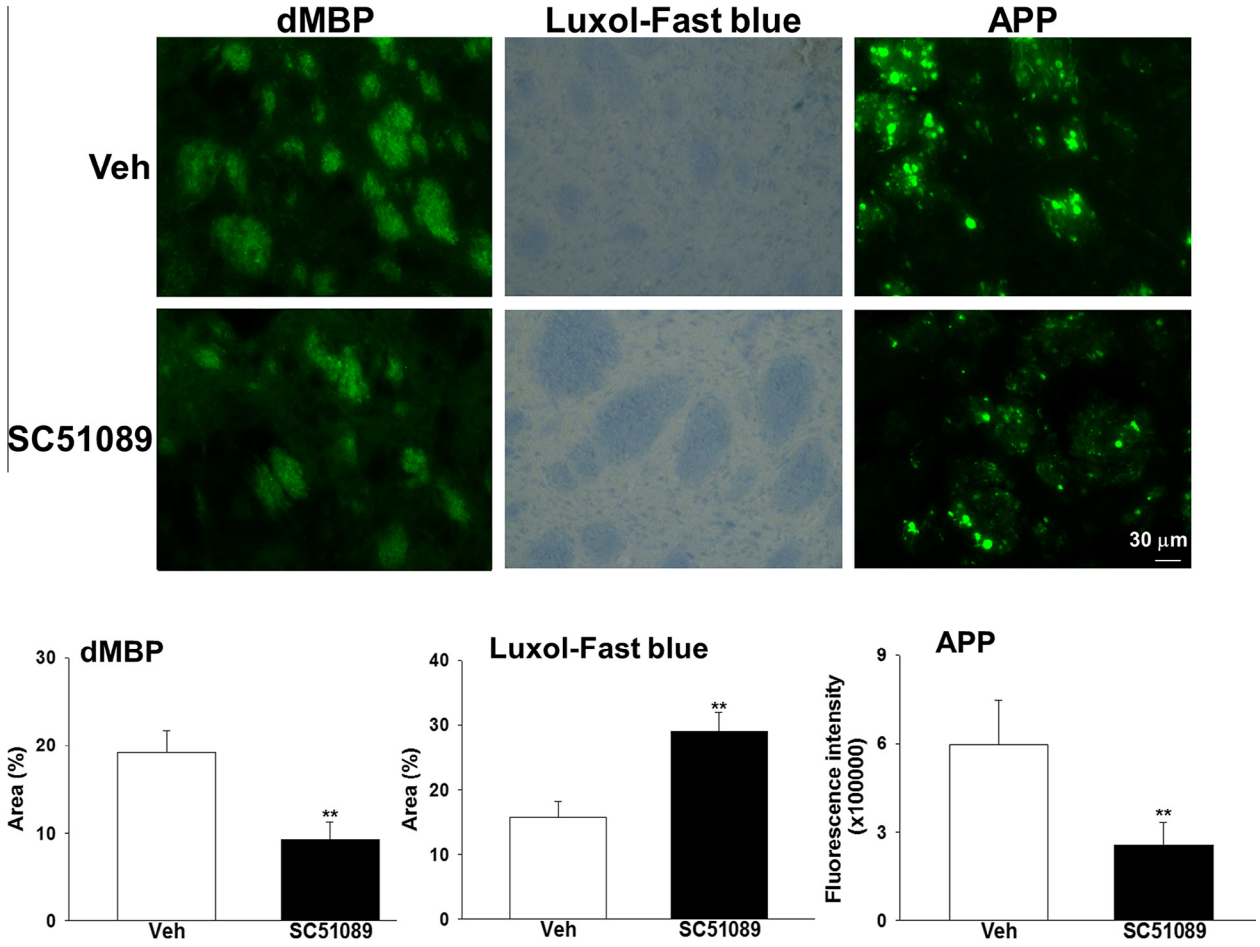

Fig. 6. Effect of EP1R inhibition on myelin and axonal damage after collagenase-induced ICH in middle-aged male mice. Representative images show dMBP-, Luxol-fast blue-, and APP-stained brain sections in the striatum of mice administered SC51089 or vehicle (Veh) on day 3 post-ICH. Scale bar: 30 μm. dMBP-labeled degraded myelin and Luxol fast blue-stained intact myelin tract were expressed as percentage of positive areas; APP-labeled damaged axons were quantified by fluorescence intensity. Bar graphs indicate that SC51089 alleviated myelin loss (left and middle) and axonal fragmentation (right). Values are mean ± SD; $n = 6$ mice/group. $^{**}p < 0.01$ vs. vehicle group.

3.3. EP1R inhibition reduces brain injury in aged male mice and middle-aged female mice after collagenase-induced ICH and in middle-aged male mice after blood- or thrombin-induced ICH

Compared with the effects of vehicle treatment, EP1R inhibition by SC51089 reduced brain injury volume (from 13.2 ± 1.0 mm^3 to 10.7 ± 0.9 mm^3), brain water content, and neurologic deficit score on days 1 and 3 in aged male mice (all $p < 0.05$; $n = 5, 5, 10$ mice/group, respectively; Fig. 4C–E) and middle-aged female mice (all $p < 0.05$; $n = 6, 5, 8$ mice/group, respectively; Fig. 4F–H) after collagenase-induced ICH. Notably, the lesion volume in aged male mice (Fig. 4C) was greater than that in the middle-aged male mice (Fig. 3B, $p < 0.05$),

EP1R inhibition by SC51089 also reduced brain water content and neurologic deficit score, and improved corner turn test performance after blood-induced ICH (all $p < 0.05$ vs. vehicle treatment; $n = 8, 12, 12$, respectively; Fig. 5A–C). The neuroprotective effect of EP1R inhibition by SC51089 was further confirmed by using primary neurons. Lactate dehydrogenase release was decreased in hemoglobin-exposed primary neurons concurrently treated with SC51089 for 24 h ($p < 0.05$; $n = 3$ per group; Fig. 5D). EP1R inhibition also reduced brain water content and neurologic deficit score on day 1 after thrombin-induced ICH (both $p < 0.05$ vs. vehicle treatment; $n = 8, 12$, respectively; Fig. 5E and F). These results confirm that EP1R inhibition protects against direct blood toxicity and thrombin toxicity.

3.4. EP1R inhibition reduces white matter injury and brain atrophy and improves long-term functional outcome after collagenase-induced ICH

Mice with ICH exhibited marked white matter injury (Wu et al., 2012). On day 3 post-ICH, we used dMBP, Luxol fast blue, and APP staining to label degraded myelin, normal myelin, and damaged axons in brain sections from mice that had been treated with SC51089 or vehicle. SC51089 post-treatment reduced myelin loss and immunostaining of dMBP and APP (all $p < 0.01$, $n = 6$ mice/group; Fig. 6), indicating reduced demyelination and axon loss in the striatum.

Next, we applied MRI to track lesion evolution on days 3 and 28 post-ICH in mice treated with SC51089 or vehicle. Compared to results in the vehicle group, EP1R inhibition by SC51089 reduced brain lesion volume on days 3 ($p < 0.01$) and 28 ($p < 0.05$) after collagenase injection ($n = 6$ mice/group; Fig. 7A). Moreover, on day 28,

Please cite this article in press as: Zhao, X., et al. Toxic role of prostaglandin E_2 receptor EP1 after intracerebral hemorrhage in mice. Brain Behav. Immun. (2015), http://dx.doi.org/10.1016/j.bbi.2015.02.011

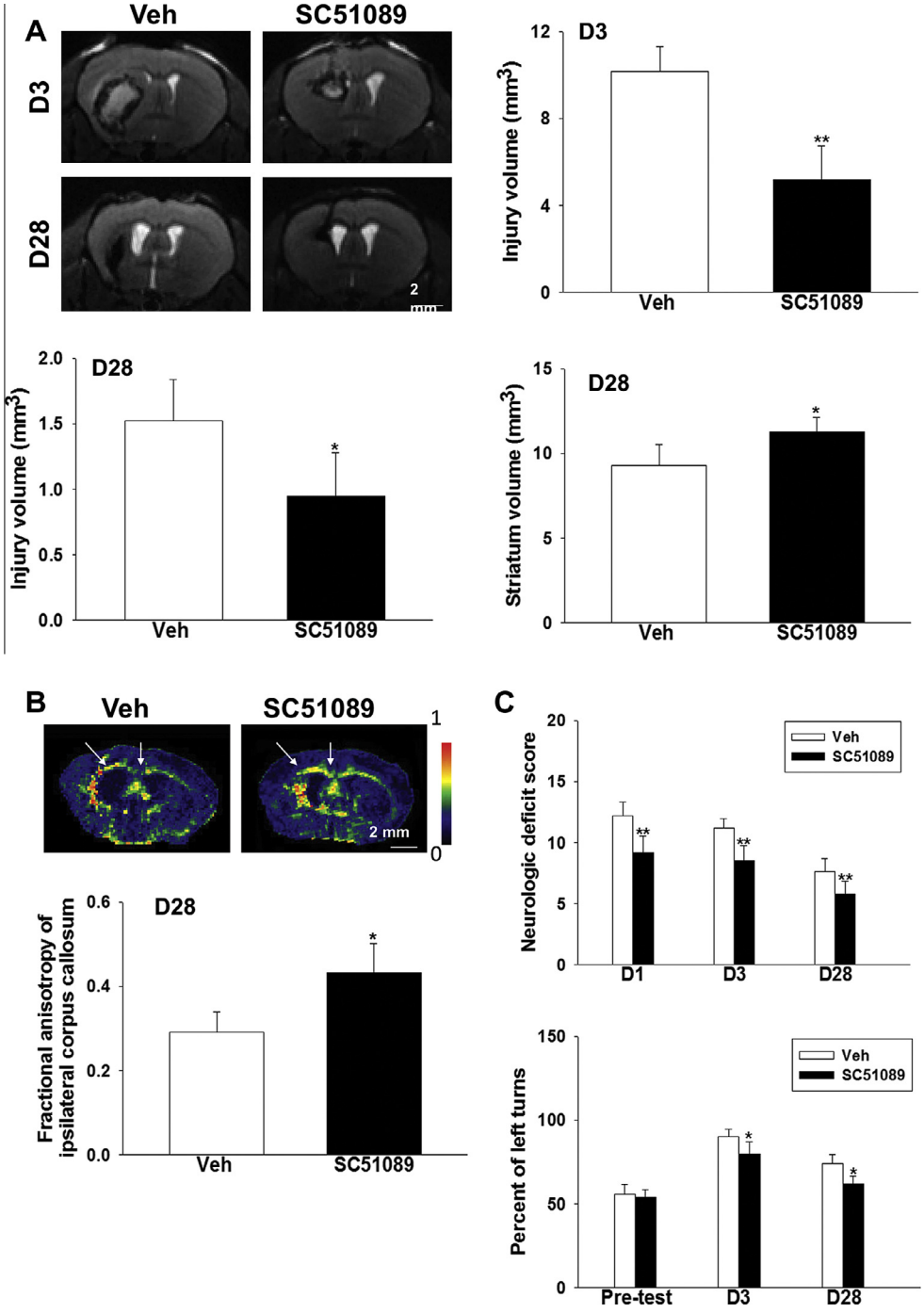

Fig. 7. Effect of EP1R inhibition on brain injury volume, brain atrophy, and white matter injury in middle-aged male mice subjected to collagenase-induced ICH. (A) Representative magnetic resonance T2* images show injury evolution in the same animals on days 3 (D3) and 28 (D28) post-ICH. Scale bar: 2 mm. Quantification analysis shows that mice treated with SC51089 had less brain injury volume than did vehicle (Veh)-treated mice on days 3 and 28 post-ICH and greater striatum volume on day 28. (B) Representative fractional anisotropy images show white matter injury of the ipsilateral corpus callosum on day 28 post-ICH. The arrows indicate the segment of corpus callosum measured. Scale bar: 2 mm. Quantification analysis shows that SC51089 administration preserved fractional anisotropy of the ipsilateral corpus callosum on day 28 post-ICH. Values are mean ± SD; $n = 6$ mice/group. (C) Compared with vehicle treatment, SC51089 treatment decreased neurologic deficit score on days 1, 3, and 28 and improved corner turn test performance on days 3 and 28 post-ICH ($n = 10$ mice/group). Values are mean ± SD. $^{*}p < 0.05$; $^{**}p < 0.01$ vs. vehicle group.

SC51089-treated mice exhibited less striatal tissue loss ($p < 0.05$) and white matter injury ($p < 0.05$) than did vehicle-treated mice, as measured by fractional anisotropy of ipsilateral corpus callosum ($n = 6$ mice/group; Fig. 7B). The improvement in neurologic function after SC51089 post-treatment was sustained up to day 28 post-ICH ($p < 0.01$ or $p < 0.05$; $n = 10$ mice/group; Fig. 7C).

3.5. EP1R inhibition reduces whereas EP1R activation increases cell death and neuronal degeneration after collagenase-induced ICH

Because EP1R inhibition produced neuroprotection by reducing brain injury and improving functional outcomes, we investigated whether this benefit is reflected on the cellular level. In the

Please cite this article in press as: Zhao, X., et al. Toxic role of prostaglandin E_2 receptor EP1 after intracerebral hemorrhage in mice. Brain Behav. Immun. (2015), http://dx.doi.org/10.1016/j.bbi.2015.02.011

vehicle-treated group, cells positive for PI and FJB were evident in the perihematomal region on day 3 after ICH. Mice post-treated with DI-004 had more PI-positive ($F = 119.76$, $p < 0.05$) and FJB-positive cells ($F = 29.88$, $p < 0.05$) than did the vehicle-treated mice, and mice post-treated with SC51089 had fewer PI-positive and FJB-positive cells (both $p < 0.05$; $n = 6$ mice/group; Fig. 8A). Similarly, DI-004 increased caspase-3 cleavage, whereas SC51089 decreased cleavage in the brain on day 1 after ICH ($F = 81.30$, all $p < 0.05$; $n = 6$ mice/group; Fig. 8B). These data support the histologic findings.

3.6. EP1R inhibition mitigates whereas EP1R activation exacerbates central and peripheral innate immune cell activation after collagenase-induced ICH

After ICH, microglia and astrocytes are activated in the perihematomal region, and neutrophils are the first infiltrating cells (Wang, 2010; Wang and Dore, 2007b). By using a combination of morphologic criteria and a cell body diameter cutoff of 7.5 μm, we classified microglia as either resting or activated (Batchelor et al., 1999; Wang et al., 2008). As expected, DI-004 increased the number of activated microglia, astrocytes, and infiltrating neutrophils compared with vehicle treatment on day 3 post-ICH ($F = 35.07$, 87.23, 50.81, respectively, all $p < 0.05$ vs. the vehicle-treated group; $n = 6$ mice/group; Fig. 9). Conversely, SC-51089 reduced the numbers of these inflammatory cells (all $p < 0.05$ vs. the vehicle-treated group; $n = 6$ mice/group; Fig. 9).

3.7. EP1R inhibition attenuates oxidative stress after collagenase-induced ICH

As early as minutes after ICH, the extravasated blood components impose a prooxidative insult that can cause neuronal death in the surrounding brain tissue (Wang, 2010; Wang and Dore, 2007b; Wang et al., 2007). We used the fluorescent indicator hydroethidine to examine superoxide production (Wu et al., 2011a). We also assessed protein carbonylation and nitrosylation. EP1R inhibition with SC51089 reduced superoxide production (small red particles) in the perihematomal region ($p < 0.05$; $n = 8$ mice/group; Fig. 10A) and reduced the level of carbonylated and nitrosylated proteins in the ICH brain ($F = 62.13$, 187.65, respec-

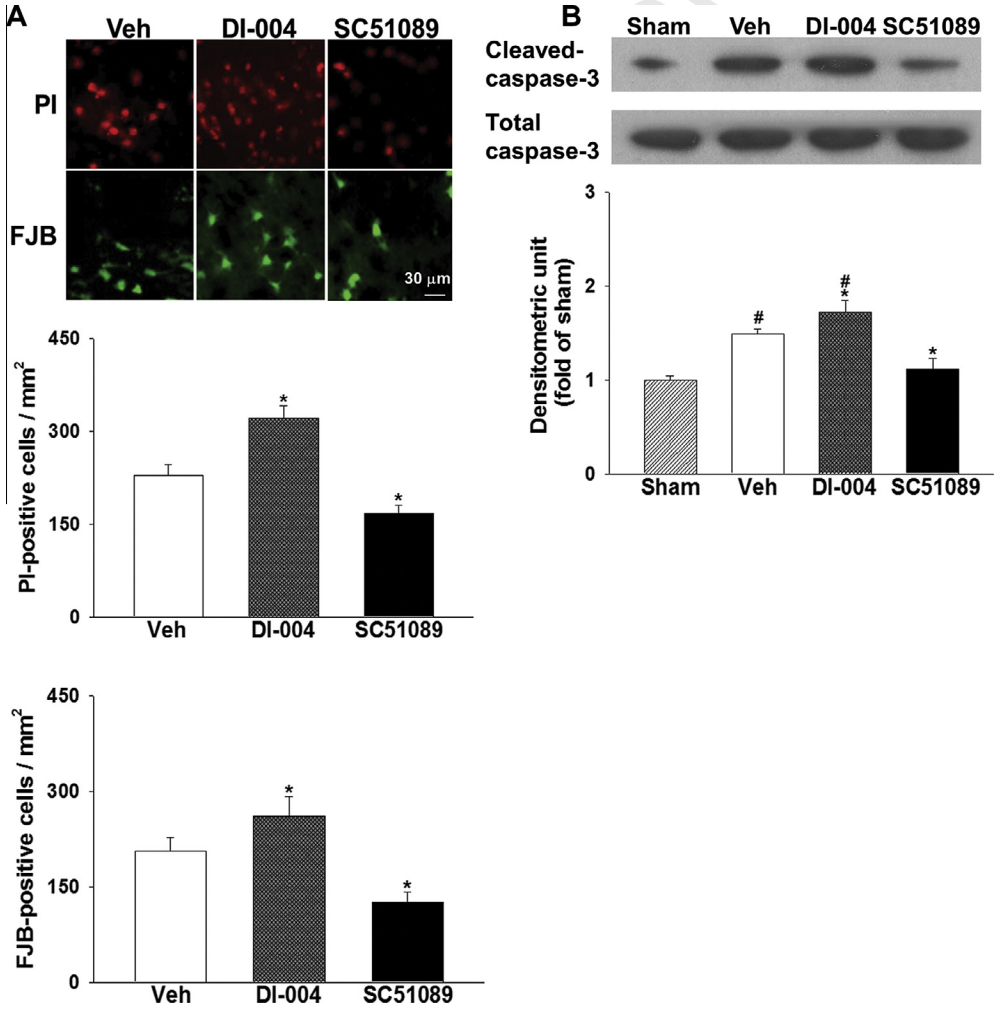

Fig. 8. Effect of EP1R activation and inhibition on cell death and neuronal degeneration in middle-aged male mice subjected to collagenase-induced ICH. (A) Representative PI- and FJB-stained brain sections on day 3 after ICH. Quantification analysis shows that the numbers of PI-positive cells and FJB-positive degenerating neurons in the perihematomal region were increased by DI-004 and decreased by SC51089 ($n = 6$ mice/group). Scale bar: 30 μm. (B) Western blot analysis and bar graph show that the level of caspase-3 cleavage in the hemorrhagic brain tissue was increased by DI-004 and decreased by SC51089 on day 1 after ICH ($n = 6$ mice/group). Values are mean ± SD. $^{\#}p < 0.05$ vs. sham group; $^{*}p < 0.05$ vs. vehicle (Veh) group.

Please cite this article in press as: Zhao, X., et al. Toxic role of prostaglandin E_2 receptor EP1 after intracerebral hemorrhage in mice. Brain Behav. Immun. (2015), http://dx.doi.org/10.1016/j.bbi.2015.02.011

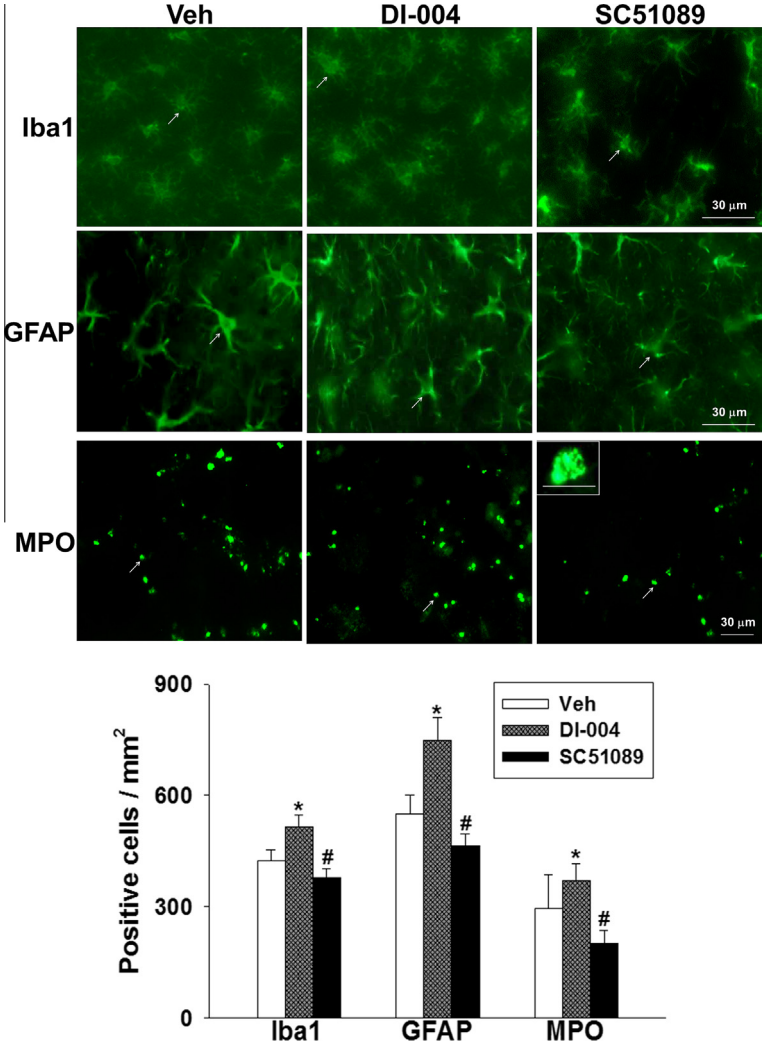

Fig. 9. Effect of EP1R activation and inhibition on glial cell activation and neutrophil infiltration in middle-aged male mice subjected to collagenase-induced ICH. In representative images, Iba1, GFAP, and MPO immunopositive cells (indicated by arrows) are evident around the hematoma on day 3 post-ICH. Scale bar: 30 μm. Inset represents an MPO-positive cell at higher magnification (scale bar = 10 μm). Quantification analysis shows that the numbers of activated microglia/macrophages, astrocytes, and infiltrating neutrophils were increased in mice that received DI-004 after ICH and decreased in those that received SC51089, compared to numbers in the vehicle (Veh)-treated group. Values are mean ± SD; $n = 6$ mice/group. $^{*}p < 0.05$ vs. vehicle group; $^{\#}p < 0.05$ vs. vehicle group.

tively, both $p < 0.05$; $n = 8$ mice/group; Fig. 10B and C), compared to that in the vehicle-treated group on day 1 post-ICH.

3.8. EP1R activation increases whereas EP1R inhibition decreases Src kinase phosphorylation after collagenase-induced ICH

To elucidate the underlying molecular mechanisms, we examined the Src kinase pathway after EP1R activation or inhibition by using the Src kinase inhibitor PP2. On day 1 post-ICH, we observed an increase in brain Src phosphorylation that was increased by DI-004. As expected, PP2 blocked the increase in Src phosphorylation ($F = 35.11$, $p < 0.05$; $n = 6$ mice/group; Fig. 11A). Importantly, EP1R inhibition by SC51089 also blocked the ICH-induced increase in Src phosphorylation ($F = 61.49$, $p < 0.05$; $n = 6$ mice/group; Fig. 11A). These data suggest that the Src kinase pathway contributes to EP1R-mediated toxicity in the hemorrhagic brain.

3.9. EP1R inhibition reduces MMP-9 activity through Src kinase signaling after collagenase-induced ICH

An increase in MMP-9 activity contributes to blood–brain barrier disruption and brain edema after ICH (Wang, 2010; Wang and Dore, 2007b; Wang and Tsirka, 2005a) and could be a critical downstream effector of Src signaling. Therefore, we examined gelatinolytic (MMP-2/9) activity in brain tissue by gelatin gel zymography, and in fresh-frozen brain sections by *in situ* zymography. In vehicle-treated mice, the activity of MMP-9, but not of MMP-2, was increased on day 1 post-ICH. DI-004 exacerbated this ICH-induced increase in MMP-9 activity, but PP2 blocked the DI-004 – induced increase ($F = 765.18$, all $p < 0.05$; $n = 6$ mice/group; Fig. 11B). As with Src phosphorylation, EP1R inhibition by SC51089 decreased the ICH-induced increase in MMP-9 activity in both gelatin gel zymography ($F = 234.40$, $p < 0.01$; $n = 6$ mice/group; Fig. 11B) and gelatin *in situ* zymography ($p < 0.05$; $n = 6$ mice/group; Fig. 11C) assays. EP1R inhibition by SC51089 also decreased MMP-9 activity after thrombin-induced ICH ($F = 10.81$, $p < 0.05$; $n = 6$ mice/group; Supplementary Fig. 4).

3.10. Src kinase signaling mediates EP1R toxicity after collagenase-induced ICH

To further confirm the role of Src kinase in EP1R-induced ICH toxicity, we administered PP2 to DI-004- or SC51089-treated mice and assessed several sets of histologic and functional outcomes after ICH induced by collagenase. On day 3 post-ICH, EP1R activa-

Please cite this article in press as: Zhao, X., et al. Toxic role of prostaglandin E_2 receptor EP1 after intracerebral hemorrhage in mice. Brain Behav. Immun. (2015), http://dx.doi.org/10.1016/j.bbi.2015.02.011

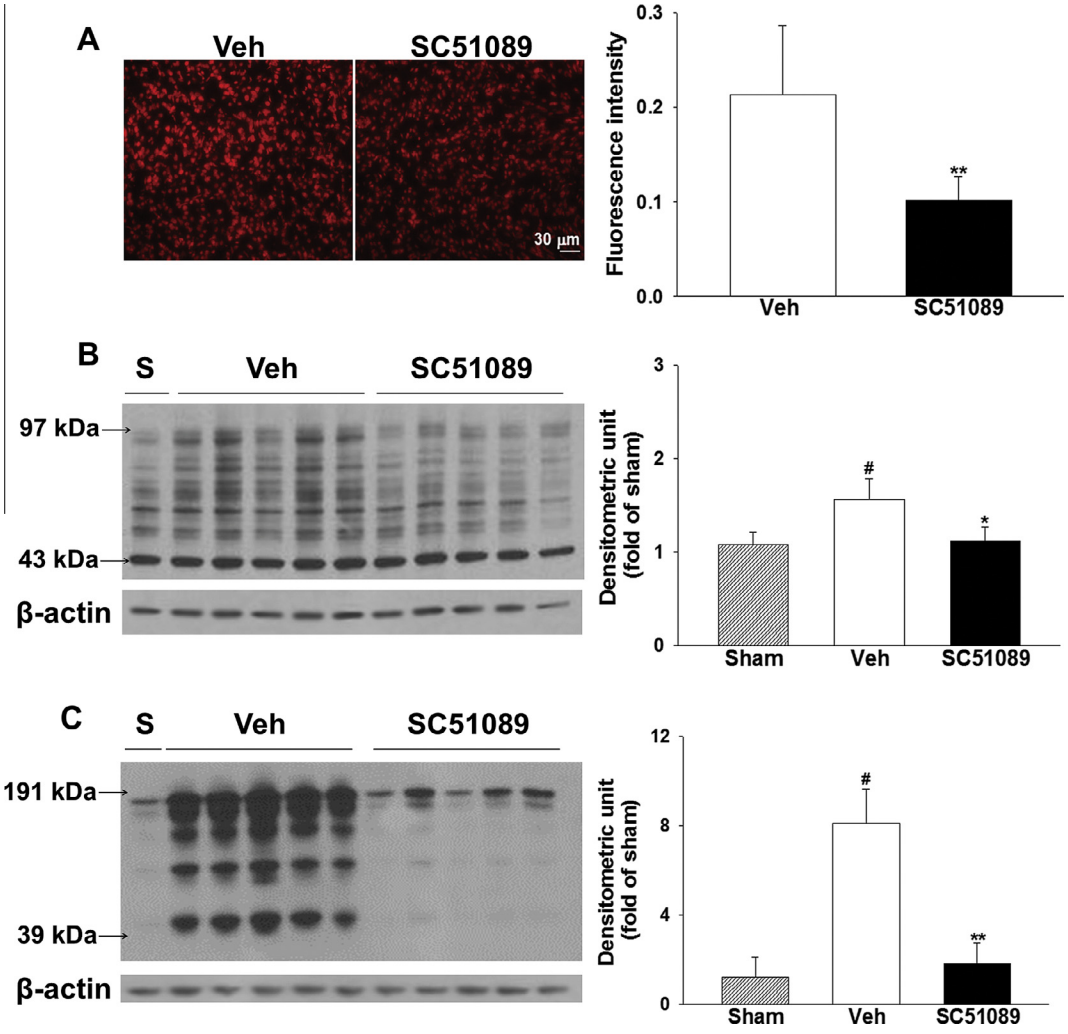

Fig. 10. Effect of EP1R inhibition on oxidative stress in middle-aged male mice subjected to collagenase-induced ICH. (A) Ethidium fluorescence (red particles), a marker for superoxide production, was evident in the perihematomal region on day 1 post-ICH. Scale bar: 30 μm. Quantification of fluorescence intensity indicated that SC51089 significantly reduced superoxide production in the perihematomal region compared to that in the vehicle (Veh)-treated group, $n = 8$ mice/group. (B and C) Representative immunoblots of hemorrhagic brain tissue and quantification analysis show that SC51089 decreased the levels of protein carbonylation (B) and nitrosylation (C) compared to those in the vehicle-treated groups on day 1 post-ICH. Optical density was integrated over multiple protein bands for carbonyls (43–97 kDa) and nitrotyrosine (39–191 kDa), $n = 8$ mice/group. β-actin served as a loading control. Values are mean ± SD; $^{\#}p < 0.05$ vs. sham group; $^{*}p < 0.05$, $^{**}p < 0.01$ vs. vehicle group. (For interpretation of the references to color in this figure legend, the reader is referred to the web version of this article.)

tion by DI-004 increased ICH-induced brain injury volume ($F = 64.71$, $n = 6$ mice/group), brain water content ($F = 10.48$, $n = 8$ mice/group), neurologic deficits ($F = 123.27$, 99.16 for days 1 and 3, respectively, $n = 12$ mice/group), cell death ($F = 50.48$, $n = 6$ mice/group), and neuronal degeneration ($F = 6.85$, $n = 6$ mice/group) compared to those in the vehicle-treated group (all $p < 0.05$; Fig. 12A–F). All of these deficits were reversed by PP2 treatment (all $p < 0.05$; Fig. 12A–F). Moreover, SC51089 and PP2, when administered separately, each decreased brain water content in the striatum ($F = 12.30$, $n = 8$ mice/group) and reduced neurologic deficit score ($F = 5.81$, $n = 12$ mice/group) on day 3 after ICH. However, when PP2 was administered to SC51089-treated mice, the brain water content ($n = 8$ mice/group) and neurologic deficits ($n = 12$ mice/group) were not further reduced (both $p > 0.05$; Fig. 12G and H). These data suggest that Src kinase signaling may contribute to EP1R-mediated toxicity after ICH.

4. Discussion

This work presents several novel findings: (1) In the striatum of the ICH brain, EP1R is expressed primarily in neurons and axons, not in astrocytes or Cx3cr1^{+} microglia; (2) in middle-aged male mice subjected to the collagenase ICH model, EP1R activation exacerbates ICH-induced brain injury, cell death, neuronal degeneration, neuroinflammation, and neurobehavioral deficits. EP1R inhibition mitigates these negative effects and has a therapeutic window of 12 h; (3) EP1R inhibition is also protective in middle-aged female mice and aged male mice and in the ICH models induced by blood or thrombin; (4) EP1R inhibition reduces oxidative stress, white matter injury, and brain atrophy and improves long-term functional outcomes; (5) EP1R activation increases, whereas its inhibition decreases, Src kinase phosphorylation and MMP-9 activity—EP1R regulates MMP-9 activity through Src kinase signaling; (6) Src kinase signaling mediates EP1R toxicity. Together, these findings suggest that EP1R activation promotes toxicity after ICH through mechanisms that involve the Src kinases and MMP-9 signaling pathway.

PGE_2 EP receptors mediate excitotoxicity and ischemic brain injury (Andreasson, 2010a,b; Jones et al., 2009), but their role in ICH is unknown. Using middle-aged and aged mice subjected to three ICH-related models (collagenase, blood, and thrombin) to avoid translational pitfalls (Kirkman et al., 2011; Wang, 2010),

Please cite this article in press as: Zhao, X., et al. Toxic role of prostaglandin E_2 receptor EP1 after intracerebral hemorrhage in mice. Brain Behav. Immun. (2015), http://dx.doi.org/10.1016/j.bbi.2015.02.011

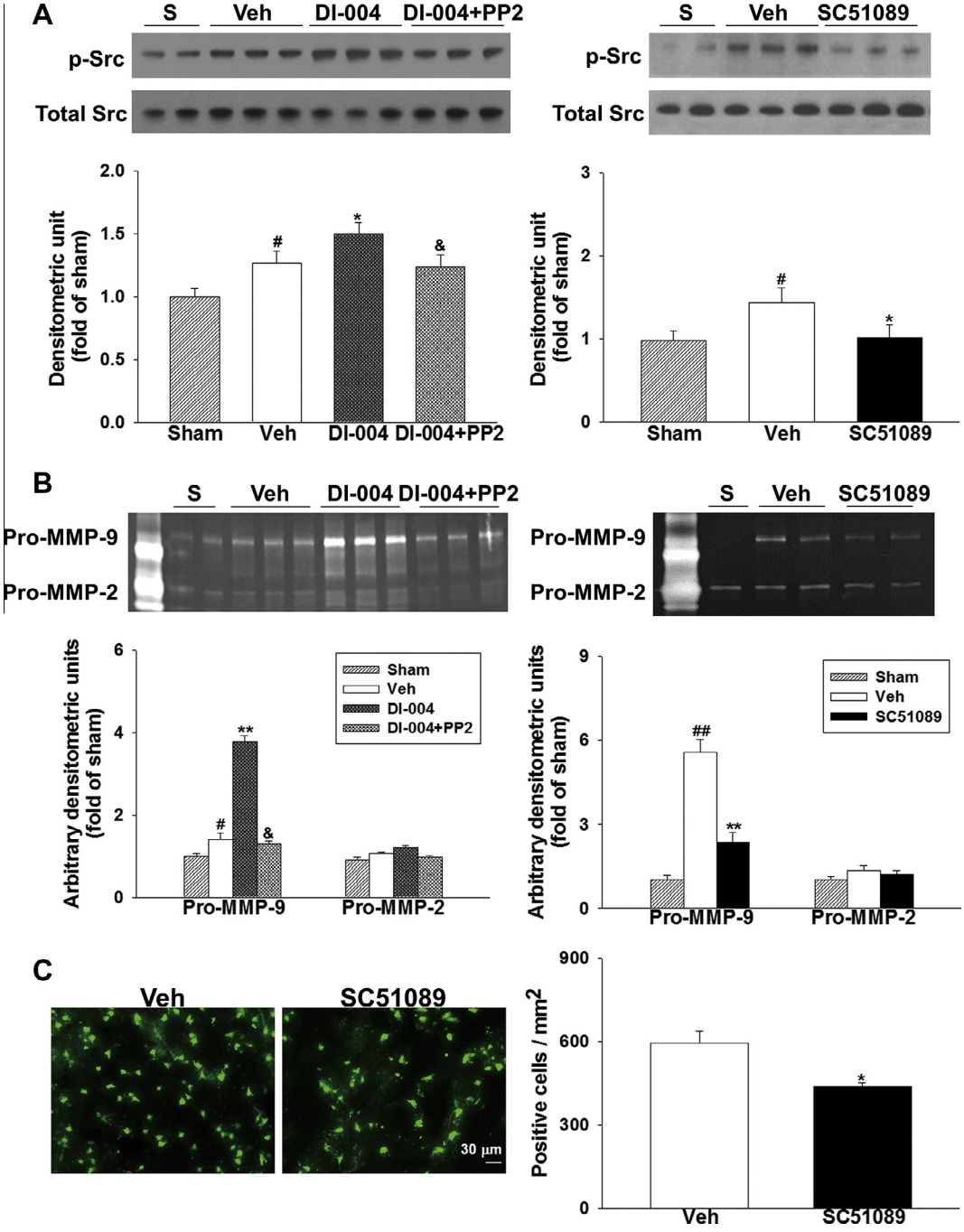

Fig. 11. Effect of EP1R inhibition on Src kinase phosphorylation and MMP-2/9 activity in middle-aged male mice subjected to collagenase-induced ICH. (A) Representative immunoblot on day 1 post-ICH shows protein levels of phosphorylated Src (p-Src) and total Src in sham-operated mice (S) and ICH mice treated with vehicle (Veh), DI-004, DI-004 + PP2, or SC51089. Densitometric analysis shows that ICH induced Src phosphorylation and that DI-004 further increased Src phosphorylation in the hemorrhagic brain. The increase in Src phosphorylation was reversed by Src kinase inhibitor PP2 and by SC51089, $n = 6$ mice/group. (B) Representative gelatin gel zymographs of MMP-2 and MMP-9 activity from sham, vehicle-, DI-004-, DI-004 + PP2-, and SC51089-treated mice on day 1 post-ICH. Quantification analysis shows that DI-004 increased the gelatinolytic activity of pro-MMP-9. PP2 and SC51089 each reversed the increase of pro-MMP-9 activity in the brain, $n = 6$ mice/group. (C) Representative gelatin *in situ* zymography fluorescent images from vehicle- and SC51089-treated mice. Scale bar: 30 μm. Quantification analysis shows that gelatinolytic activity was lower in SC51089-treated mice than in vehicle-treated mice on day 1 post-ICH, $n = 6$ mice/group. Values are mean ± SD; $^{\#}p < 0.05$, $^{\#\#}p < 0.01$ vs. sham group; $^{*}p < 0.05$, $^{**}p < 0.01$ vs. vehicle group; $^{\&}p < 0.05$ vs. DI-004 group.

we confirmed the toxic role of EP1R activation after ICH. Although sex differences and aging influence stroke outcomes and response to drug treatment (Fisher et al., 2009; Hurn et al., 2005), only a few ICH studies have been conducted in female and aged animals. We demonstrated here that the neuroprotective effect of EP1R inhibition after ICH is also present in middle-aged females and aged males.

One limitation of ICH research is that most preclinical studies have focused only on mechanisms of gray matter injury. In contrast, our knowledge of white matter injury remains limited. White matter injury is often associated with a higher risk of death and poor functional outcome in stroke patients (Leys et al., 1999). Indeed, white matter injury was identified as a priority for both basic and clinical ICH research at the 2003 National Institute of

Please cite this article in press as: Zhao, X., et al. Toxic role of prostaglandin E_2 receptor EP1 after intracerebral hemorrhage in mice. Brain Behav. Immun. (2015), http://dx.doi.org/10.1016/j.bbi.2015.02.011

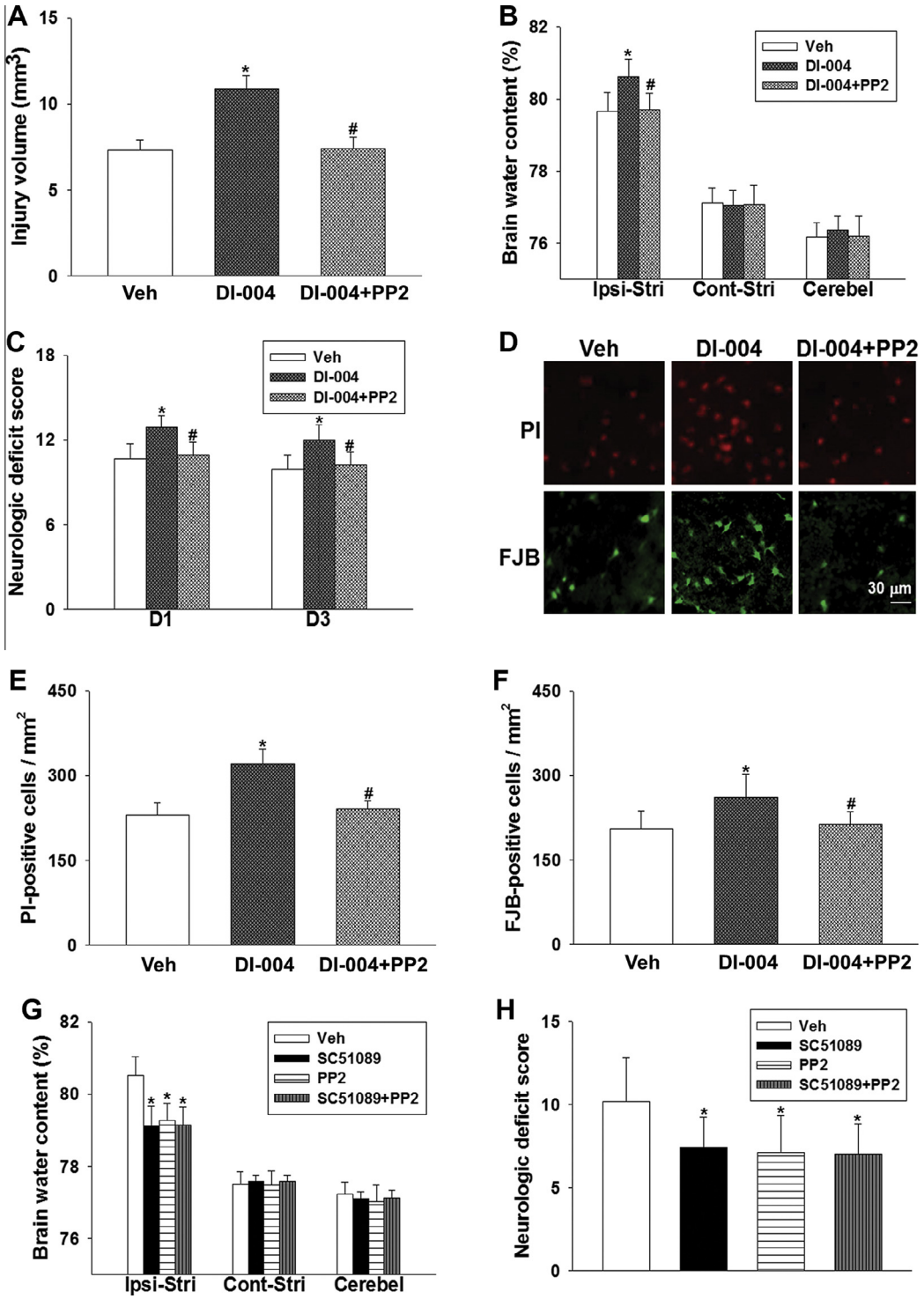

Fig. 12. Src kinase inhibition mitigates EP1R-mediated toxicity in middle-aged male mice subjected to collagenase-induced ICH. (A–C) Bar graphs show that EP1R activation by DI-004 increased brain injury volume (A; $n = 6$ mice/group), brain water content (B; $n = 8$ mice/group), and neurologic deficit score (C; $n = 12$ mice/group) on day 3 post-ICH. Src kinase inhibitor PP2 blocked these increases. (D) Representative PI- and FJB-stained brain sections from mice on day 3 after collagenase-induced ICH and treatment with vehicle (Veh), DI-004, or DI-004 + PP2. (E and F) Quantification analysis shows that DI-004 increased PI-positive cells (E; $n = 6$ mice/group) and FJB-positive degenerating neurons (F; $n = 6$ mice/group) in the perihematomal regions. PP2 treatment blocked these increases. (G and H) Bar graphs show that ICH-induced increases in brain water content (G; $n = 8$ mice/group) and neurologic deficit score (H; $n = 12$ mice/group) were decreased on day 3 in SC51089-treated and PP2-treated mice. Co-treatment with SC51089 and PP2 did not further decrease these values. Values are mean ± SD; $^{*}p < 0.05$ vs. vehicle-treated group; $^{\#}p < 0.05$ vs. DI-004-treated group. Ipsi-Stri, ipsilateral striatum; Cont-Stri, contralateral striatum; Cerebel, cerebellum.

Neurological Disorders and Stroke Intracerebral Hemorrhage workshop (2005). Since that time, only a few studies (Moxon-Emre and Schlichter, 2011; Wasserman and Schlichter, 2008), including our own (Wu et al., 2012), have investigated white matter injury in rodent ICH models, and only at early time points. No study has focused on white matter tracts during recovery after ICH. Although MRI has been used for ICH research in rats for years (Belayev et al., 2007; Brown et al., 1995; Del Bigio et al., 1996;

Please cite this article in press as: Zhao, X., et al. Toxic role of prostaglandin E_2 receptor EP1 after intracerebral hemorrhage in mice. Brain Behav. Immun. (2015), http://dx.doi.org/10.1016/j.bbi.2015.02.011

MacLellan et al., 2008; Okauchi et al., 2010; Strbian et al., 2007), it is used mainly to determine the hematoma volume. MRI, especially DTI, can be used to monitor white matter damage (Mori and Zhang, 2006). DTI has been used to identify white matter injury and recovery after stroke, traumatic brain injury, and several other diseases in rodents (Jiang et al., 2011, 2010; Zhang et al., 2012), but it has not been applied to ICH research in rodents. To our knowledge, this study is the first to investigate gray and white matter damage and recovery in mouse ICH models by three approaches: histology, immunohistochemistry, and MRI/DTI. Immunohistochemistry and histology showed that EP1R was expressed in the fiber tracts of the corpus callosum and that EP1R inhibition reduced demyelination and axonal loss. MRI/DTI confirmed histologic results and showed that EP1R inhibition reduced injury volume, white matter injury, and brain atrophy. The results also suggest that MRI/DTI can be used to evaluate gray and white matter damage and recovery in mouse ICH models.

In rodents (Wang et al., 2003; Wang and Tsirka, 2005b; Zhu et al., 2012) and humans (Wang et al., 2011), the major forms of cell death after ICH are necrosis and apoptosis. In the perihematomal region of rodents, the number of necrotic and apoptotic cells peaks at 72 h post-ICH (Matsushita et al., 2000; Zhu et al., 2012). The attenuation of cell and neuronal degeneration conferred by EP1R inhibition, as evidenced by reductions in PI staining, FJB staining, and cleaved caspase-3, is consistent with our *in vitro* study showing that SC51089 decreases the death of neurons exposed to hemoglobin. These data suggest that EP1R inhibition has a direct protective effect on neurons. Similar results were reported in a recent *in vitro* study in which primary neurons were treated with toxic levels of hemin (Mohan et al., 2013). Interestingly, contrary to their *in vitro* data, the same group reported that EP1 deletion exacerbates ICH outcomes *in vivo,* potentially by impairing microglial phagocytosis (Singh et al., 2013). A prior study showed that EP1R is expressed in neurons but not in microglia in the ischemic brain (Kawano et al., 2006). In the ICH brain, we found that EP1R was expressed primarily in neurons and axons, less frequently in round $CD11b^+$ cells, and rarely in typical process-bearing $CD11b^+$ microglia. Based on the fact that CD11b is a marker for both microglia and blood-borne myeloid cells and that all microglia are GFP^+ in $Cx3cr1^{GFP/+}$ mice (Cardona et al., 2006), we further confirmed that resting and reactive $Cx3cr1^+$ microglia in the perihematomal region rarely express EP1R. This finding supports the possibility that EP1R might be expressed mostly in amoeboid $CD11b^+$ myeloid cells, such as macrophages, mast cells, neutrophils, and dendritic cells, but not in microglia. Therefore, our data do not support the idea that EP1R can directly affect microglial phagocytosis *in vivo* after ICH. It will be important to determine what blood-borne myeloid cells express EP1R and the effects of EP1R deletion or inhibition on the function of EP1R-expressing myeloid cells, which might play an important role in ICH pathology.

Cellular inflammatory responses, including overactivation of microglia and astrocytes and infiltration of leukocytes and macrophages that release proinflammatory cytokines, chemokines, ROS, and other toxic mediators, contribute to ICH-induced secondary brain injury (Wang, 2010; Wang and Dore, 2007b). Consistent with this notion, we have shown previously that inhibition of microglial activation before or 2 h after ICH improves histologic and functional outcomes (Wang et al., 2003; Wang and Tsirka, 2005b). Others have shown that leukocyte depletion reduces blood–brain barrier disruption, axon injury, and inflammation after ICH (Moxon-Emre and Schlichter, 2011). In this study, we showed that EP1R activation exacerbates cellular inflammation on day 3 after ICH, whereas EP1R inhibition mitigates this inflammation; thus EP1R may target the signals that mediate cellular inflammatory response. Finally, the reduction in inflammation that we observed after EP1R inhibition was associated with reductions in ROS production and oxidative brain damage. This finding is important because reducing ROS with free radical scavengers, or by genetic deletion of the ROS-generating enzyme NADPH oxidase, reduces ICH-induced brain damage in mice (Nakamura et al., 2008; Tang et al., 2005). To minimize the concern that increases or decreases in cell death, cellular inflammatory responses, and ROS production are due to differences in lesion volume, we performed profile-based cell counting in vehicle and treatment groups using brain sections with similar-sized hematomas.

Increased Src kinase activity contributes to ischemic stroke injury (Paul et al., 2001; Zan et al., 2011, 2014) and thrombin-induced cell death (Ardizzone et al., 2007; Liu et al., 2010, 2008). However, the link between EP1R and Src kinases has not been established in ICH models. It is well known that Src and other Src family kinases are abundant in neurons (Kalia et al., 2004). We showed here that EP1R is present mostly in neurons in the ICH brain. Therefore, the interaction between EP1R and Src should also occur in the neurons. The phosphorylation state of Src kinase is altered by EP1R activation or inhibition, suggesting that Src could be a downstream target of EP1R. The fact that EP1R antagonist SC51089 and Src inhibitor PP2 did not have an additive effect further supports the sequential pathway of EP1R and Src signaling. In this regard, the increase in lesion volume in EP1R knockout mice after ICH (Singh et al., 2013) might be caused by chronic inhibition of Src signaling, which has the opposite effect of acute inhibition (Liu and Sharp, 2011). These opposing effects could also explain the contradictory findings from EP1R knockout mice (Singh et al., 2013) and mice with acute inhibition of EP1R, as we report here.

Although MMP-9 might be a downstream target of Src kinase signaling (Liu and Sharp, 2011), a direct connection has not been established. We showed for the first time that, in the collagenase-induced ICH model, Src kinase signaling regulates MMP-9 activity and mediates EP1R toxicity. Consistent with these findings, we and others have shown that MMP-9 inhibition or deletion is neuroprotective after ICH (Wang and Tsirka, 2005a; Xue et al., 2009a,b). The molecular mechanism by which Src kinase signaling regulates MMP-9 activity after ICH remains to be defined.

Our study provides proof of concept that EP1R inhibition has neuroprotective effects with clinical implications for patients with ICH. However, we need to establish whether EP1R inhibition is also effective in higher species, such as piglets and monkeys, and whether sex differences affect the ICH outcomes conferred by EP1R inhibition. Furthermore, PGE_2 acts through receptors EP1–4, and the synergistic or antagonistic effects of EP1R with other EP receptors must be defined. Although we have tested SC51089 in our *in vivo* and *in vitro* ICH models, more selective EP1R antagonists are available (Jones et al., 2009), and their neuroprotective potency needs to be systematically evaluated.

In summary, we provide the first preclinical evidence that PGE_2 EP1R plays a toxic role after ICH through mechanisms that involve the Src kinases and the MMP-9 signaling pathway. Hence, EP1R inhibition could be developed as a novel therapeutic strategy to reduce inflammatory injury and improve functional outcomes after ICH.

Conflicts of interest

The authors declare no competing financial interests.

Acknowledgments

This work was supported by AHA 13GRNT15730001, NIH K01AG031926, R01NS078026, and R01AT007317 (JW). We thank Suzy Cho, Lingshu Liu, Joy Ziyi Zhou, Weizhu Tang, and Jieru

UNCORRECTED PROOF

Wan for blind analysis of histology and immunofluorescence and for neuronal culture. We thank Claire Levine, MS, ELS, for assistance with manuscript preparation and Dr. Raymond Koehler, Dr. Zengjin Yang, and the Wang lab team members for insightful input.

Appendix A. Supplementary data

Supplementary data associated with this article can be found, in the online version, at http://dx.doi.org/10.1016/j.bbi.2015.02.011.

References

Abe, T., Kunz, A., Shimamura, M., Zhou, P., Anrather, J., Iadecola, C., 2009. The neuroprotective effect of prostaglandin E2 EP1 receptor inhibition has a wide therapeutic window, is sustained in time and is not sexually dimorphic. J. Cereb. Blood Flow Metab. 29, 66–72.

Ahmad, A.S., Saleem, S., Ahmad, M., Doré, S., 2006. Prostaglandin EP1 receptor contributes to excitotoxicity and focal ischemic brain damage. Toxicol. Sci. 89, 265–270.

Andreasson, K., 2010a. Emerging roles of PGE2 receptors in models of neurological disease. Prostaglandins Other Lipid Mediat. 91, 104–112.

Andreasson, K., 2010b. Prostaglandin signalling in cerebral ischaemia. Br. J. Pharmacol. 160, 844–846.

Ardizzone, T.D., Zhan, X., Ander, B.P., Sharp, F.R., 2007. SRC kinase inhibition improves acute outcomes after experimental intracerebral hemorrhage. Stroke 38, 1621–1625.

Batchelor, P.E., Liberatore, G.T., Wong, J.Y., Porritt, M.J., Frerichs, F., Donnan, G.A., Howells, D.W., 1999. Activated macrophages and microglia induce dopaminergic sprouting in the injured striatum and express brain-derived neurotrophic factor and glial cell line-derived neurotrophic factor. J. Neurosci. 19, 1708–1716.

Belayev, L., Obenaus, A., Zhao, W., Saul, I., Busto, R., Wu, C., Vigdorchik, A., Lin, B., Ginsberg, M.D., 2007. Experimental intracerebral hematoma in the rat: characterization by sequential magnetic resonance imaging, behavior, and histopathology. Effect of albumin therapy. Brain Res. 1157, 146–155.

Brown, M.S., Kornfeld, M., Mun-Bryce, S., Sibbitt, R.R., Rosenberg, G.A., 1995. Comparison of magnetic resonance imaging and histology in collagenase-induced hemorrhage in the rat. J. Neuroimaging 5, 23–33.

Cardona, A.E., Pioro, E.P., Sasse, M.E., Kostenko, V., Cardona, S.M., Dijkstra, I.M., Huang, D., Kidd, G., Dombrowski, S., Dutta, R., Lee, J.C., Cook, D.N., Jung, S., Lira, S.A., Littman, D.R., Ransohoff, R.M., 2006. Control of microglial neurotoxicity by the fractalkine receptor. Nat. Neurosci. 9, 917–924.

Chang, C.F., Chen, S.F., Lee, T.S., Lee, H.F., Chen, S.F., Shyue, S.K., 2011. Caveolin-1 deletion reduces early brain injury after experimental intracerebral hemorrhage. Am. J. Pathol. 178, 1749–1761.

Chang, C.F., Cho, S., Wang, J., 2014. (−)-Epicatechin protects hemorrhagic brain via synergistic Nrf2 pathways. Ann. Clin. Transl. Neurol. 1, 258–271.

Chu, K., Jeong, S.W., Jung, K.H., Han, S.Y., Lee, S.T., Kim, M., Roh, J.K., 2004. Celecoxib induces functional recovery after intracerebral hemorrhage with reduction of brain edema and perihematomal cell death. J. Cereb. Blood Flow Metab. 24, 926–933.

Del Bigio, M.R., Yan, H.J., Buist, R., Peeling, J., 1996. Experimental intracerebral hemorrhage in rats. Magnetic resonance imaging and histopathological correlates. Stroke 27, 2312–2319, discussion 2319–2320.

Fisher, M., Feuerstein, G., Howells, D.W., Hurn, P.D., Kent, T.A., Savitz, S.I., Lo, E.H., 2009. Update of the stroke therapy academic industry roundtable preclinical recommendations. Stroke 40, 2244–2250.

Fukumoto, K., Takagi, N., Yamamoto, R., Moriyama, Y., Takeo, S., Tanonaka, K., 2010. Prostanoid EP1 receptor antagonist reduces blood-brain barrier leakage after cerebral ischemia. Eur. J. Pharmacol. 640, 82–86.

Gong, C., Ennis, S.R., Hoff, J.T., Keep, R.F., 2001. Inducible cyclooxygenase-2 expression after experimental intracerebral hemorrhage. Brain Res. 901, 38–46.

Hurn, P.D., Vannucci, S.J., Hagberg, H., 2005. Adult or perinatal brain injury: does sex matter? Stroke 36, 193–195.

Jiang, Q., Qu, C., Chopp, M., Ding, G.L., Davarani, S.P., Helpern, J.A., Jensen, J.H., Zhang, Z.G., Li, L., Lu, M., Kaplan, D., Hu, J., Shen, Y., Kou, Z., Li, Q., Wang, S., Mahmood, A., 2011. MRI evaluation of axonal reorganization after bone marrow stromal cell treatment of traumatic brain injury. NMR Biomed. 24, 1119–1128.

Jiang, Q., Zhang, Z.G., Chopp, M., 2010. MRI evaluation of white matter recovery after brain injury. Stroke 41, S112–S113.

Jones, R.L., Giembycz, M.A., Woodward, D.F., 2009. Prostanoid receptor antagonists: development strategies and therapeutic applications. Br. J. Pharmacol. 158, 104–145.

Kalia, L.V., Gingrich, J.R., Salter, M.W., 2004. Src in synaptic transmission and plasticity. Oncogene 23, 8007–8016.

Kawano, T., Anrather, J., Zhou, P., Park, L., Wang, G., Frys, K.A., Kunz, A., Cho, S., Orio, M., Iadecola, C., 2006. Prostaglandin E_2 EP1 receptors: downstream effectors of COX-2 neurotoxicity. Nat. Med. 12, 225–229.

Keep, R.F., Hua, Y., Xi, G., 2012. Intracerebral haemorrhage: mechanisms of injury and therapeutic targets. Lancet Neurol. 11, 720–731.

Kirkman, M.A., Allan, S.M., Parry-Jones, A.R., 2011. Experimental intracerebral hemorrhage: avoiding pitfalls in translational research. J. Cereb. Blood Flow Metab. 31, 2135–2151.

Leys, D., Englund, E., Del Ser, T., Inzitari, D., Fazekas, F., Bornstein, N., Erkinjuntti, T., Bowler, J.V., Pantoni, L., Parnetti, L., De Reuck, J., Ferro, J., Bogousslavsky, J., 1999. White matter changes in stroke patients. Relationship with stroke subtype and outcome. Eur. Neurol. 42, 67–75.

Liu, D.Z., Ander, B.P., Xu, H., Shen, Y., Kaur, P., Deng, W., Sharp, F.R., 2010. Blood–brain barrier breakdown and repair by Src after thrombin-induced injury. Ann. Neurol. 67, 526–533.

Liu, D.Z., Cheng, X.Y., Ander, B.P., Xu, H., Davis, R.R., Gregg, J.P., Sharp, F.R., 2008. Src kinase inhibition decreases thrombin-induced injury and cell cycle re-entry in striatal neurons. Neurobiol. Dis. 30, 201–211.

Liu, D.Z., Sharp, F.R., 2011. The dual role of SRC kinases in intracerebral hemorrhage. Acta Neurochir. Suppl. 111, 77–81.

MacLellan, C.L., Silasi, G., Poon, C.C., Edmundson, C.L., Buist, R., Peeling, J., Colbourne, F., 2008. Intracerebral hemorrhage models in rat: comparing collagenase to blood infusion. J. Cereb. Blood Flow Metab. 28, 516–525.

Matsushita, K., Meng, W., Wang, X., Asahi, M., Asahi, K., Moskowitz, M.A., Lo, E.H., 2000. Evidence for apoptosis after intercerebral hemorrhage in rat striatum. J. Cereb. Blood Flow Metab. 20, 396–404.

Mohan, S., Glushakov, A.V., Decurnou, A., Narumiya, S., Dore, S., 2013. Contribution of PGE2 EP1 receptor in hemin-induced neurotoxicity. Front. Mol. Neurosci. 6, 31.

Mori, S., Zhang, J., 2006. Principles of diffusion tensor imaging and its applications to basic neuroscience research. Neuron 51, 527–539.

Moxon-Emre, I., Schlichter, L.C., 2011. Neutrophil depletion reduces blood–brain barrier breakdown, axon injury, and inflammation after intracerebral hemorrhage. J. Neuropathol. Exp. Neurol. 70, 218–235.

Nakamura, T., Kuroda, Y., Yamashita, S., Zhang, X., Miyamoto, O., Tamiya, T., Nagao, S., Xi, G., Keep, R.F., Itano, T., 2008. Edaravone attenuates brain edema and neurologic deficits in a rat model of acute intracerebral hemorrhage. Stroke 39, 463–469.

NINDS ICH Workshop Participants, 2005. Priorities for clinical research in intracerebral hemorrhage: report from a National Institute of Neurological Disorders and Stroke workshop. Stroke 36, e23–e41.

Okauchi, M., Hua, Y., Keep, R.F., Morgenstern, L.B., Schallert, T., Xi, G., 2010. Deferoxamine treatment for intracerebral hemorrhage in aged rats: therapeutic time window and optimal duration. Stroke 41, 375–382.

Paul, R., Zhang, Z.G., Eliceiri, B.P., Jiang, Q., Boccia, A.D., Zhang, R.L., Chopp, M., Cheresh, D.A., 2001. Src deficiency or blockade of Src activity in mice provides cerebral protection following stroke. Nat. Med. 7, 222–227.

Singh, N., Ma, B., Leonardo, C.C., Ahmad, A.S., Narumiya, S., Dore, S., 2013. Role of PGE(2) EP1 receptor in intracerebral hemorrhage-induced brain injury. Neurotox. Res. 24, 549–559.

Strbian, D., Tatlisumak, T., Ramadan, U.A., Lindsberg, P.J., 2007. Mast cell blocking reduces brain edema and hematoma volume and improves outcome after experimental intracerebral hemorrhage. J. Cereb. Blood Flow Metab. 27, 795–802.

Tang, J., Liu, J., Zhou, C., Ostanin, D., Grisham, M.B., Neil Granger, D., Zhang, J.H., 2005. Role of NADPH oxidase in the brain injury of intracerebral hemorrhage. J. Neurochem. 94, 1342–1350.

Tober, K.L., Wilgus, T.A., Kusewitt, D.F., Thomas-Ahner, J.M., Maruyama, T., Oberyszyn, T.M., 2006. Importance of the EP(1) receptor in cutaneous UVB-induced inflammation and tumor development. J. Invest. Dermatol. 126, 205–211.

Wang, J., 2010. Preclinical and clinical research on inflammation after intracerebral hemorrhage. Prog. Neurobiol. 92, 463–477.

Wang, J., Dore, S., 2007a. Heme oxygenase-1 exacerbates early brain injury after intracerebral haemorrhage. Brain 130, 1643–1652.

Wang, J., Dore, S., 2007b. Inflammation after intracerebral hemorrhage. J. Cereb. Blood Flow Metab. 27, 894–908.

Wang, J., Fields, J., Dore, S., 2008. The development of an improved preclinical mouse model of intracerebral hemorrhage using double infusion of autologous whole blood. Brain Res. 1222, 214–221.

Wang, J., Fields, J., Zhao, C., Langer, J., Thimmulappa, R.K., Kensler, T.W., Yamamoto, M., Biswal, S., Dore, S., 2007. Role of Nrf2 in protection against intracerebral hemorrhage injury in mice. Free Radic. Biol. Med. 43, 408–414.

Wang, J., Rogove, A.D., Tsirka, A.E., Tsirka, S.E., 2003. Protective role of tuftsin fragment 1–3 in an animal model of intracerebral hemorrhage. Ann. Neurol. 54, 655–664.

Wang, J., Tsirka, S.E., 2005a. Neuroprotection by inhibition of matrix metalloproteinases in a mouse model of intracerebral haemorrhage. Brain 128, 1622–1633.

Wang, J., Tsirka, S.E., 2005b. Tuftsin fragment 1–3 is beneficial when delivered after the induction of intracerebral hemorrhage. Stroke 36, 613–618.

Wang, J., Zhuang, H., Dore, S., 2006. Heme oxygenase 2 is neuroprotective against intracerebral hemorrhage. Neurobiol. Dis. 22, 473–476.

Wang, Y.X., Yan, A., Ma, Z.H., Wang, Z., Zhang, B., Ping, J.L., Zhu, J.S., Zhou, Y., Dai, L., 2011. Nuclear factor-kappaB and apoptosis in patients with intracerebral hemorrhage. J. Clin. Neurosci. 18, 1392–1395.

Wasserman, J.K., Schlichter, L.C., 2008. White matter injury in young and aged rats after intracerebral hemorrhage. Exp. Neurol. 214, 266–275.

Wu, H., Wu, T., Li, M., Wang, J., 2012. Efficacy of the lipid-soluble iron chelator 2, 2′-dipyridyl against hemorrhagic brain injury. Neurobiol. Dis. 45, 388–394.

UNCORRECTED PROOF

Wu, H., Wu, T., Xu, X., Wang, J., Wang, J., 2011. Iron toxicity in mice with collagenase-induced intracerebral hemorrhage. J. Cereb. Blood Flow Metab. 31, 1243–1250.

Wu, H., Zhang, Z., Hu, X., Zhao, R., Song, Y., Ban, X., Qi, J., Wang, J., 2010. Dynamic changes of inflammatory markers in brain after hemorrhagic stroke in humans: a postmortem study. Brain Res. 1342, 111–117.

Wu, T., Wu, H., Wang, J., Wang, J., 2011. Expression and cellular localization of cyclooxygenases and prostaglandin E synthases in the hemorrhagic brain. J. Neuroinflammation 8, 22.

Xue, M., Fan, Y., Liu, S., Zygun, D.A., Demchuk, A., Yong, V.W., 2009a. Contributions of multiple proteases to neurotoxicity in a mouse model of intracerebral haemorrhage. Brain 132, 26–36.

Xue, M., Hollenberg, M.D., Demchuk, A., Yong, V.W., 2009b. Relative importance of proteinase-activated receptor-1 versus matrix metalloproteinases in intracerebral hemorrhage-mediated neurotoxicity in mice. Stroke 40, 2199–2204.

Zan, L., Wu, H., Jiang, J., Zhao, S., Song, Y., Teng, G., Li, H., Jia, Y., Zhou, M., Zhang, X., Qi, J., Wang, J., 2011. Temporal profile of Src, SSeCKS, and angiogenic factors after focal cerebral ischemia: correlations with angiogenesis and cerebral edema. Neurochem. Int. 58, 872–879.

Zan, L., Zhang, X., Xi, Y., Wu, H., Song, Y., Teng, G., Li, H., Qi, J., Wang, J., 2014. Src regulates angiogenic factors and vascular permeability after focal cerebral ischemia-reperfusion. Neuroscience 262, 118–128.

Zhang, J., Aggarwal, M., Mori, S., 2012. Structural insights into the rodent CNS via diffusion tensor imaging. Trends Neurosci. 35, 412–421.

Zhu, W., Gao, Y., Chang, C.F., Wan, J.R., Zhu, S.S., Wang, J., 2014. Mouse models of intracerebral hemorrhage in ventricle, cortex, and hippocampus by injections of autologous blood or collagenase. PLoS ONE 9, e97423.

Zhu, X., Tao, L., Tejima-Mandeville, E., Qiu, J., Park, J., Garber, K., Ericsson, M., Lo, E.H., Whalen, M.J., 2012. Plasmalemma permeability and necrotic cell death phenotypes after intracerebral hemorrhage in mice. Stroke 43, 524–531.

UNCORRECTED PROOF

Please cite this article in press as: Zhao, X., et al. Toxic role of prostaglandin E_2 receptor EP1 after intracerebral hemorrhage in mice. Brain Behav. Immun. (2015), http://dx.doi.org/10.1016/j.bbi.2015.02.011